MICROFLUIDIC DEVICES FOR THE CHARACTERIZATION AND MANIPULATION OF ENCAPSULATED CELLS IN AGAROSE MICROCAPSULES USING DIELECTROPHORESIS AND ELECTROPHORESIS

ADEFEMI HABIB ADEYEMI

Thesis submitted to the Faculty of Graduate and Postdoctoral Studies
in partial fulfillment of the requirements for

Master of Applied Science – Biomedical Engineering

FACULTY OF ENGINEERING
UNIVERSITY OF OTTAWA

ABSTRACT

Cell encapsulation is a promising concept in regenerative medicine and stem cell treatment of diseases. Cells encapsulated in hydrogels have shown to yield better therapeutic outcome over cells in suspension. Microfluidic platforms have facilitated the process of cell encapsulation through the controlled mixing of aqueous cell solution and hydrogel with an immiscible liquid to yield a monodispersed population of microcapsules at a high throughput. However, given that the microfluidic process of placing cells in microcapsules is completely random, yielded samples are often riddled with empty microcapsules, raising the need for a post-encapsulation purification step to sort empty microcapsules from cell-laden ones. Sorting of microcapsules can be achieved through several techniques, most desirable of which are electrokinetic such as dielectrophoresis (DEP) and electrophoresis (EP). The advantages of DEP and EP techniques are that they support label-free sorting and yield a high throughput. However to achieve true effective DEP or EP sorting, there is a need to understand how empty microcapsules react to these electrokinetic forces versus occupied microcapsules. This study developed microfluidic devices for characterising the electrokinetic effects on microcapsules using DEP and EP. Results of both characterization techniques showed notable differences in the response of empty microcapsules versus cell-laden ones, reinforcing their potentials for sorting. Furthermore, this study proposed designs for microcapsules sorting devices that leverage EP and DEP.

STATEMENT OF ORIGINALITY

The content presented in this document is the product of original work performed by the author at the University of Ottawa under the supervision of Professor Michel Godin.

In partial fulfillment of the requirements for the degree of Master of Science (Physics) at the University of Ottawa, this work was presented at the Ottawa Carleton Institute for Biomedical Engineering Seminar Series:

Adefemi H. Adeyemi and Michel Godin, *Microfluidic Device for High Throughput Sorting of Encapsulated Cells in Agarose Microcapsules using Dielectrophoresis*. Ottawa Carleton Institute for Biomedical Engineering, March 2017.

A poster on the same topic was also presented at the Solutions for Cardio-pulmonary Organ Repair and Regeneration (SCORR) Scientific Research Day:

Adefemi H. Adeyemi and Michel Godin, *Microfluidic Device for High Throughput Sorting of Encapsulated Cells in Agarose Microcapsules using Dielectrophoresis*. Solutions for Cardio-pulmonary Organ Repair and Regeneration (SCORR) Scientific Research Day, March 2017.

STATEMENT OF CONTRIBUTIONS

The entirety of this document was written by the author. All figures and tables were created by the author unless otherwise mentioned in the caption. The work presented were largely performed by the author including, photomask designs, fabrication of devices (photolithography, wet etching, PDMS mould replication), testing of devices, electrical setup for DEP and EP experiments, encapsulation of cells for DEP and EP experiments, experimentation, and data collection. The cell encapsulation setup along with the Labview® code for the control of pressure regulators and heating/cooling blocks for the cell encapsulation module pictured in Figure 20 were created by Professor Michel Godin. The cell encapsulation device mentioned in Chapter 3 (Figure 19) was designed by Nicolas Monette-Catafard with added modifications by Dr. Ainara Benavente-Babace. The first generation DEP sorting device mentioned in Chapter 5 (Figure 32a) was designed by Dr. Benjamin Watts but fabricated and tested by the author. Cell culturing was performed by the author with occasional help from Dr. Ainara Benavente-Babace.

ACKNOWLEDGEMENTS

TABLE OF CONTENTS

LIST OF FIGURES

Chapter 1

INTRODUCTION

Cell encapsulation involves the seclusion of single or multiple cells within individual spherical picolitre-sized micro-compartments known as microcapsules [1]. The concept has been shown to improve the therapeutic outcome of stem cell treatments as stem cells encapsulated in hydrogels such as agarose have proven to engraft and persist better than stem cells in suspension post-transplant [2]. Cell engraftment and persistence, once encapsulated cells are introduced into a patient, are some of the biggest challenges in most cell-based therapies.

Micro-environments for cells are typically created in hydrogel droplets. These droplets are often inert in nature and thus do not interact chemically with cells, and are permeable which allows for the exchange of nutrients and gases between cells and their environment [3]. Also, the hydrogel membrane allows for the outward and inward diffusion of small signalling proteins such as cytokines which are secreted by the enclosed cells [4]. Cytokines and other signalling proteins are important in the context of cell encapsulation because they facilitate intercellular communication between individually isolated cells to promote certain cellular functions [5]. Essentially, microcapsules are able to provide an environment that sustains regular cellular activities, such as metabolism, proliferation, and differentiation while allowing enclosed cells to integrate into the target tissue [6].

Cell encapsulation primarily emerged as a way to protect stem cells from immune attacks during transplantation without resorting to the use of risk-prone immune suppressing drugs [6]. By enclosing cells in the safety of gelled microcapsule cocoons, a physical barrier is created that shields them from the harmful reach of the immune system/antibodies which might consider them as foreign invaders to be destroyed [4]. This in turn facilitates their long term survival and their ultimate chances of realising their intended therapeutic functions. The efficiency of cell encapsulation has been demonstrated in

studies investigating treatments of several human conditions including anaemia [7], renal failure [8], diabetes [9], hemophilia [10], and ischemic cardiomyopathy [2].

Pertinent to the advancement of cell encapsulation as a clinical modality in the treatment of diseases is the technique of encapsulation itself. Formation of cell-laden microcapsules have traditionally followed two approaches: emulsification and extrusion [11]. Emulsification involves the creation of emulsions by agitating an aqueous cell solution mixed with hydrogel in an immiscible organic medium such as oil. Extrusion on the other hand involves squeezing out droplets of cell mixture with hydrogels through thin needles. Both techniques are considered impractical to meet certain important requirements such as high throughput, monodispersity of microcapsules, and high cell occupancy rate [12].

To yield a monodispersed population of encapsulated cells for clinical relevance at high throughputs, there is need for a better control of the encapsulation process. Microfluidic technologies have enabled better manipulation of samples to achieve a high throughput and monodispersed microcapsules. Exceptionally uniformly sized microcapsules can be generated using microfluidic-based devices at throughputs of over 10 kHz, less than 3% of which are polydispersed [13]. This is possible given the advantages that microfluidics offers such as small fluidic channel sizes and ease of automation of the encapsulation process.

Even though microfluidics has greatly improved the problems of throughput and monodispersity, the issue of low to moderate occupancy rate still largely lingers. The distribution of cells into microcapsules is random, and governed by Poisson Ratio [1]. The probability of having n amount of cells enclosed in a single microcapsule if the mean number of cells per microcapsule (λ) is known is predicted by [14]:

$$P_n = \frac{\lambda^n e^{-\lambda}}{n}$$

(1)

Consequently, the chances of having microcapsules that are empty are considerably high (see Figure 1). A typical load concentration of 6 million cells per milliliter fed into a microfluidic device to generate monodispersed 50-picoliter microcapsules will yield 74% of microcapsules with no cells, 22% containing single cells, and the rest containing two or more cells [15].

One way to improve the occupancy rate is to increase the initial load concentration of cells. This approach however comes at the expense of potentially clogging the already narrow fluidic channel and

nozzle delivering the cell samples. Another approach is to implement an on-chip sorting module that separates and discards empty microcapsules and keep the ones containing cells.

Many microfluidics techniques of particle or cell sorting have been proposed over the years [16]. These sorting techniques have leveraged different phenomena including electrokinetic [17] [18], acoustic [19] [20], optical [21] [22], magnetic [23], and hydrodynamic [24]. Post-encapsulation sorting of cell-laden microcapsules is an area that is starting to emerge and is drawing from the body of work and progress made in the area of particle and cell sorting [14].
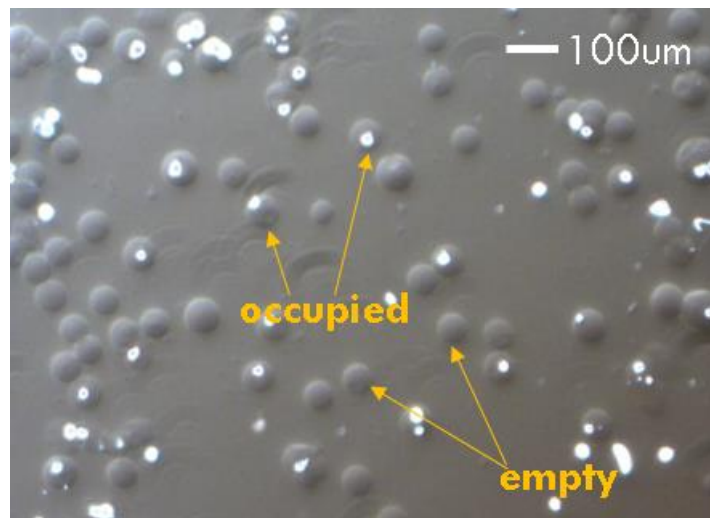
Figure 1: Phase Contrast microscope image of 3T3 mouse fibroblast cells encapsulated in 50um agarose microcapsules. Microfluidic encapsulation technique yields medium to low occupancy rate.

Electrokinetic sorting methods as an option for sorting encapsulated cells are particularly attractive compared to other methods (e.g. optical and magnetic) because they can potentially support label-free sorting [25]. That is they do not necessarily require cells to be pre-labelled with fluorescent biomarkers, antibodies, magnetic beads, or nanoparticles in order to facilitate detection – a process that can alter cellular biophysical properties and compromise their applicability for therapies [17]. In addition to the advantage of label-free sorting, electrokinetic methods can achieve high sorting throughputs and accuracies [26].

Electrokinetic sorting operates by using electric fields to exert forces on a target. The magnitude of force imparted on the target varies depending on its charge, size, dielectric properties, and so on [26]. Two of

the common electrokinetic effects used in microfluidic-based sorting are dielectrophoresis and electrophoresis. Dielectrophoresis describes the movement of a neutral or charged particle in the presence of non-uniform alternating current (AC) electric field [27]. Electrophoresis on the other hand refers to the movement of a charged particle in the presence of a uniform direct current (DC) electric field [28].

Dielectrophoresis (DEP) is a frequency dependent phenomenon, meaning that the DEP force experienced by a particle will vary over a range of frequencies. DEP force is also dependent on the unique physical attributes of the particle such as size and dielectric properties, and on the medium surrounding the particle. Frequency-dependent DEP profiles for two different particles of different dielectric makeup will be unique and different for each of those particles. A microcapsule containing cell is expected to have a different dielectric characteristic from a microcapsule that is empty, hence will likely exhibit a different DEP frequency profile at certain frequencies. If these frequencies are identified, they can be exploited to separate the microcapsule group experiencing stronger DEP forces from the one experiencing weaker DEP forces. Determining the frequency dependent DEP profile of empty microcapsules and that of occupied microcapsule is therefore an important precursor to the effective DEP sorting of microcapsules.

Electrophoresis (EP), on the other hand, is a phenomenon that depends mostly on the net charge of a particle and on the strength of applied electric field. The higher the net charge a particle possesses, the greater the electrophoretic force it experiences. It is expected that a microcapsule containing cells will have a different net charge from a microcapsule that is empty, all other conditions being the same, and will thus experience a different electrophoretic force. The difference in electrophoretic forces translates to a difference in the terminal velocities of respective EP-induced motions. These differences in EP velocities can be leveraged for sorting. Thus, performing characterization of EP velocities is an important first step towards the implementation of EP sorting of microcapsules.

Most of the studies done on DEP frequency-dependent characterization and on EP velocity characterization to date have been based on bare cells suspended in media as opposed to encapsulated cells. Lionel Broche et al [29] developed a technique for DEP characterization of cells based on DEP well electrode technology. K. Kaler and T.B. Jones [30] successfully demonstrated DEP characterization of cells in media using a feedback controlled levitation system. Witek et al showed EP velocity characterization of E.coli and baker's yeast cells using a simple microfluidic device [31].

Characterization of micro particles is a highly relevant step towards effective sorting. Knowing how empty microcapsules and ones occupied by cells behave with respect to one another under the influence of DEP or EP forces will help with the design of an effective sorting platform. To the best of my knowledge there has been no published attempt demonstrating DEP characterization of encapsulated cells to date. Neither have I come across any published attempt to characterize EP mobilities of encapsulated cells. This research thus seeks to fill this knowledge gap by implementing microfluidic techniques to characterize DEP and EP properties of microcapsules with an outlook towards sorting.

The overall goal of this Master's thesis is therefore to:

(1) propose a microfluidic device for the DEP characterization of microcapsules

(2) propose a microfluidic device for the EP characterization of microcapsules

(3) propose possible sorting methodologies for DEP and EP sorting of cell-laden microcapsules

Chapter 2 of the report gives a more complete background on the principles of microfluidics, cell encapsulation, as well as more in-depth discussions of DEP and EP theories. Chapter 3 demonstrates the characterization of DEP forces on microcapsules. Chapter 4 demonstrates the characterization of EP forces on microcapsules. Chapter 5 presents an outlook to DEP and EP sorting based on the characterizations results presented in chapters 3 and 4.

Chapter 2

BACKGROUND

2.1   Microfluidic Fundamentals

Microfluidics has enabled the simplified manipulation of fluids and particles at the micrometer scale. Common applications are seen in research involving DNA analysis, enzyme assays, cell-based assays, cytometry, cell sorting, cellular bio-sensing, and so on [28]. Microfluidic devices, characterized by networks of micrometer-wide fluidic channels, are designed with unique features tailored for specialized tasks such as mixing, measurement, sorting, trapping, and isolation. The greatest advantages that these devices offer are: (i) miniaturization – the ability to integrate multiple laboratory process into a small chip, thus conserving precious samples by using smaller volumes; (ii) parallelization – the ability to scale processes for mass production; and (iii) high throughput – the ability to speed up processes due to ease of automation.

In order to take advantage of the above listed benefits that microfluidics offer, there is a need to understand the important factors governing the operation of these devices at the micrometer level. A notable factor that affects the workings of microfluidic devices is the regime of flow inside fluidic microchannels. Another pertains to the velocity profile of flow. These two phenomena are explained in the following sections.

2.1.1   Flow Regimes in Microfluidic Devices

In order to perform the functions listed above, certain flow profiles are exploited. In a pressurized flow channel, Laminar flow and Turbulent flow are the two major types of flow profiles that dominate [28].

Laminar flow (Figure 2a) exists where fluid particles flow in a smooth orderly fashion parallel to the walls of the channel such that no mixing occurs among fluid particles by any means other than through simple diffusion. Turbulent flow (Figure 2b), on the other hand, exists where fluid particles flow in a random haphazard fashion and rapid mixing occurs.

(a) Laminar flow profile   (b) Turbulent flow profile
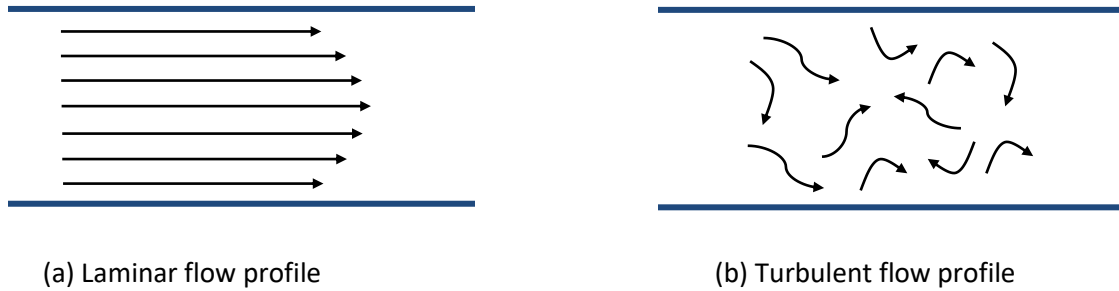
Figure 2: Illustration of the two different flow profiles in fluidic microchannels

The characteristic flow regime in a microchannel under set conditions can be predicted by a factor known as Reynolds number. Reynolds number is a dimensionless quantity that estimates the flow behavior of fluids under different conditions in a flow channel [32]. It describes the ratio between inertial forces and viscous forces acting on fluids within a channel and is given by the formula:

$$Re = \frac{\rho v l}{\mu}$$

(2)

ρ = density of the fluid (kg/m^3)

v = velocity of flow (m/s)

l = travelled length of fluid (m)

μ = dynamic viscosity of fluid (kg/m/s)

Laminar flow occurs when Re < 2300; turbulent flow occurs when Re > 4000. Between Re = 2300 and Re = 4000, there is a combination of laminar and turbulent flows, often referred to as transitional flow

[28]. It has been shown that in microfluidic devices, laminar flow is the flow profile that prevails [32] with Re numbers well below 1. This owes to the small sizes of fluidic channels.

2.1.2   Velocity Profile in Microfluidic Channels

In a pressure driven microfluidic channel where flow is laminar and the passing fluid is incompressible (i.e. fluid density is constant), the velocity of flow across channel width follows a parabolic profile where velocity field is maximum at the geometric center and tends to zero towards the channel walls (see Figure 3). This, however, assumes that there is a no-slip condition at play at the interface between the fluid and the walls of the channel. A no-slip boundary condition implies that the tangential component of fluid velocity is equal to that of the solid surface it is in contact with, therefore in a channel where the walls are motionless [33], the tangential component of fluid velocity at wall boundaries should be zero.
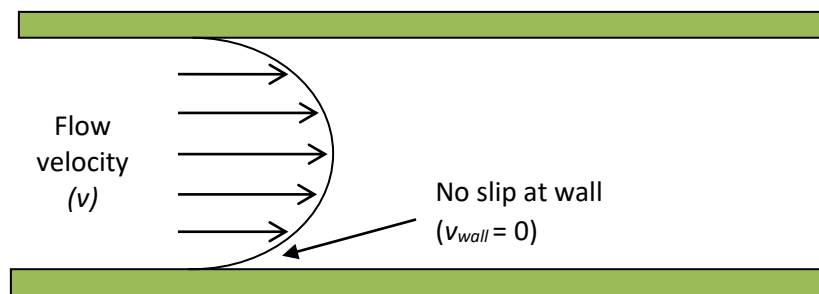
Figure 3: Illustration of velocity profile in a microchannel assuming there is a no-slip boundary condition

The Navier-Stokes equation is a very important relation in microfluidics as it governs the flow of fluids in microchannels where the passing fluid is incompressible. It originates from the application Newton's second law of motion to fluidic elements and addresses the conservation of momentum in fluidic channels. The equation is given as follow:

$$\rho \frac{\partial v}{\partial t} + \rho v \cdot \nabla v = -\nabla p + \mu \nabla^2 v + g$$

(3)

8

$\boldsymbol{v}$ = velocity vector field of fluid

$\boldsymbol{p}$ = pressure

$\boldsymbol{\rho}$ = fluid density

$\boldsymbol{\mu}$ = dynamic viscosity of fluid

$\boldsymbol{g}$ = acceleration vector by external forces

The Navier-Stokes equation is generally solved in combination with the Continuity Equation. The Continuity Equation addresses the conservation of mass in fluidic elements and is given by:

$$\frac{\partial \boldsymbol{v}}{\partial \boldsymbol{t}} + \boldsymbol{\nabla} \cdot (\boldsymbol{\rho v}) = \boldsymbol{0}$$

(4)

2.2　Fundamentals of Dielectrophoretic Force

Dielectrophoresis is a phenomenon that describes the deflection of a charged or neutral particle when subjected to a non-uniform electric field [27]. When a particle is placed in the vicinity of a non-uniform electric field, it experiences lateral forces which causes the particle to deflect. The deflection occurs as a result of the polarization effects on the particle [34]. Essentially, the electric field polarizes the particle and turns it into a dipole whereby all positive charges line up on one side and all negative charges on the other side. If the electric field is non-uniform, one side of the particle will experience a greater force than the other, and a dipole moment will be induced. The net force will either drive the particle towards the region of high electric field gradient, i.e. positive DEP, or away into region of weaker electric field gradient, i.e. negative DEP [35]. This is illustrated in the Figure 4.

The net DEP force depends on the polarization of the particle relative to the medium in which it is suspended [28]. At a set frequency of electric field, if the particle has a higher polarizability than the medium, the net DEP force is positive. On the other hand, if the medium has a higher polarizability than the particle, the net DEP force is negative.
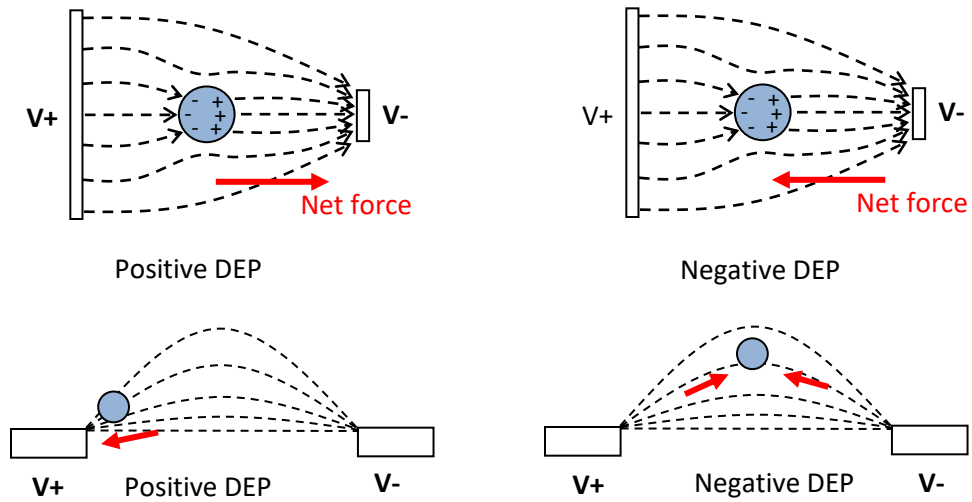
Figure 4: Illustration direction of DEP induced motion of a neutrally charged particle when subjected to non-uniform electric field

DEP force depends on a number of factors such as the size of the particle, its dielectric properties, its surrounding medium, the frequency of applied signal causing the electric field, and so on [28]. The force is described by the formula:

$$F_{DEP} = 2\pi r^3 \varepsilon_m \varepsilon_0 Re(f_{CM}) \nabla E^2$$

(5)

ε_m = relative permittivity of medium

ε_0 = permittivity of free space

r = radius of particle

$Re(f_{CM})$ = real part of Clausius-Mossoti (CM) factor

∇E^2 = electric field gradient

The Clausius-Mossotti factor is a dimensionless quantity given by:

$$f_{CM} = \frac{\varepsilon_p^* - \varepsilon_m^*}{\varepsilon_p^* + 2\varepsilon_m^*}$$

<div align="right">(6)</div>

ε_m^* = complex permittivity of medium

ε_p^* = complex permittivity of particle

The Clausius-Mossotti factor (f_{CM}) defines the relative polarizability of a particle with respect to its surrounding medium and depends on the frequency of the applied AC electric field. As shown in equation 6, Clausius-Mossotti factor is a function of the dielectric properties of the particle and the medium, given by their respective complex permittivities. Complex permittivity of a particle or medium, in turn, is determined by the frequency of the applied AC field, and the conductivity of the particle or medium as shown by equations 7.

$$\varepsilon_p^* = \varepsilon_p + j \cdot \left(\frac{\sigma_p}{2\pi f}\right); \quad \varepsilon_m^* = \varepsilon_m + j \cdot \left(\frac{\sigma_m}{2\pi f}\right)$$

<div align="right">(7)</div>

ε_p = relative permittivity of particle

ε_m = relative permittivity of medium

σ_p = conductivity of particle

σ_m = conductivity of medium

f = frequency of applied AC electric field

The real part of Claussius-Mossoti factor $Re(f_{CM})$, in theory, varies anywhere from +1 to -0.5 and dictates the overall polarity of the DEP force, i.e. whether the DEP force it is negative or positive. A positive value of Claussius-Mossoti factor indicates a positive DEP and vice versa.

2.3   Fundamentals of Electrophoretic Force

Electrophoresis is a phenomenon that describes the movement of a charged particle when subjected to a uniform DC electric field [28]. The movement occurs as a result of the electrostatic effect (Coulomb forces) acting on the particle, which drives it in the direction of the oppositely charged electrode (Figure 5). A positively charged particle will exhibit motion towards the negative electrode while a negatively charged particle will exhibit motion towards the positive electrode. The electrophoretic force exerted on a particle is proportional to the charge of the particle and the intensity of the electric field, and is predicted by Coulomb's law:

| Negatively charged particle | Positively charged particle | Neutrally charged particle |
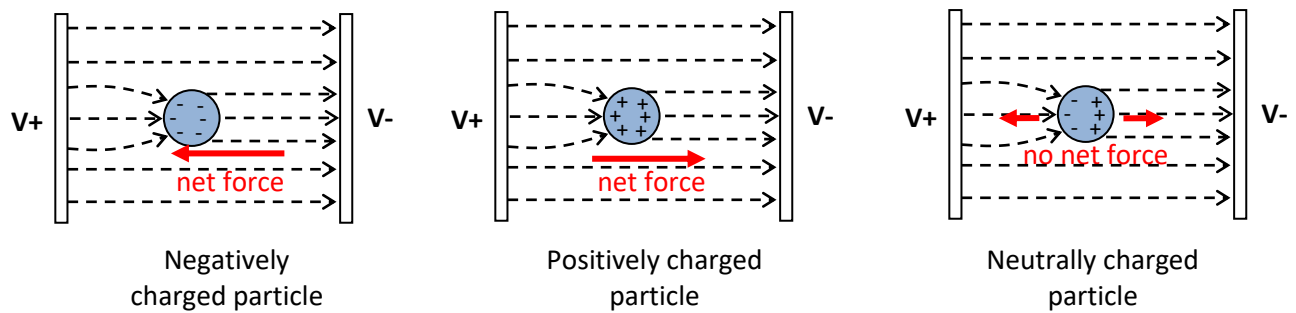
Figure 5: Illustration of EP movement of a particle relative to an applied DC electric field

$$F_{EP} = qE$$

(8)

q = net charge of particle

E = applied electric field

And the electric field is given by:

$$E = \frac{V}{d}$$

(8)

V = applied voltage

d = distance between electrodes

2.4　Fundamentals of Microfluidic Cell Encapsulation

Microfluidics allows for the miniaturization of the encapsulation process allowing for the use of smaller volumes of reagents and for a better control of the encapsulation process [13]. By using hydrodynamic pumping, reagents, aqueous cell solution + hydrogel and oil are delivered into a microfluidic chip with specially designed microchannels that facilitates mixing, and consequently formation of monodispersed aqueous droplets or microcapsules. The size of droplets can be tuned by adjusting the channel geometry and the hydrodynamic pressure at which reagents are pumped. These processes are explained in details in the following sub-sections.

2.4.1　Droplet Generation

Critical to the concept of microfluidics cell encapsulation is the formation of the aqueous droplets. These droplets, when generated with a suitable hydrogel, form microcapsules in which cells can be suspended. There are two different techniques commonly used in microfluidics for generating droplets: T-junction and Flow focusing [36]. These two techniques utilise different microchannel geometries to control the interaction of an aqueous phase with an immiscible phase resulting in the formation of droplets. They are passive in nature and continuously produce streams of monodispersed droplets as long as the fluidic channels remain suitably pressurized. The formation of droplets in these two techniques generally require the collision of two streams of flow: an aqueous phase which will be formed into droplets, also known as the dispersed phase; and an immiscible phase (typically some kind of oil) which surrounds and carries the droplets, also known as the continuous phase. The shear force of collision of the continuous phase with the dispersed phase pinches the flow of the dispersed phase and causes it to break off into a dispersed stream of droplets. The device geometry for each of the technique is described as follow.

T-junction

This technique was first demonstrated by Thorsen, et al in 2001 [37]. As its name implies, it utilises a microchannel design in the shape of the letter 'T'. The dispersed phase flows through the stem channel and intersects with the continuous phase which flows through the main channel as shown in Figure 6. This technique is more stable at low flow rates and thus more favourable for the formation of monodispersed droplets for applications where a low flow rate is desired.
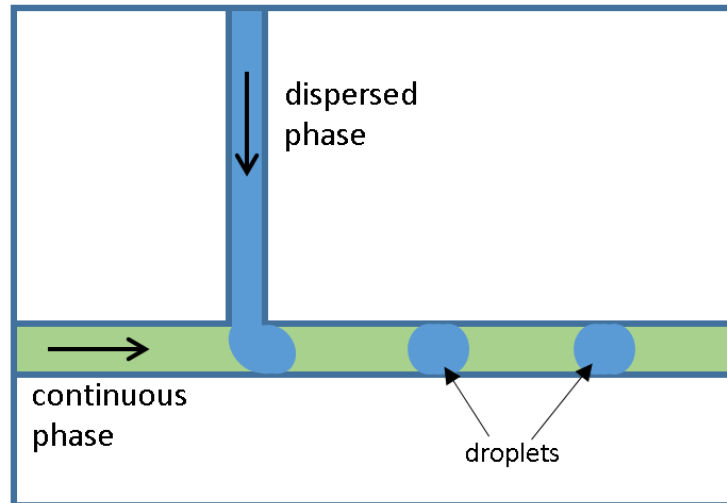
Figure 6: T-junction channel design for droplet formation

Flow Focusing

This technique was first demonstrated by Anna et al in 2003 [38]. Here the microchannel design consists of three inlet channels converging at an intersection and then leading into an outlet channel as shown in Figure 7. The middle inlet channel carries the dispersed phase and is intersected at an angle of 90 degree by two side inlet channel that are carrying the continuous phase. The direction of flow in all three inlet channels is towards the intersection. This technique is ideal for continuous production of monodispersed droplets at a high throughput of up to 10 kHz.
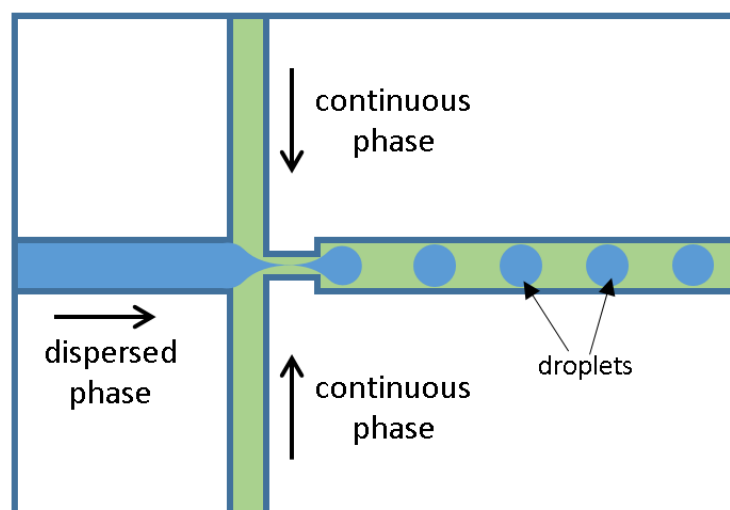
Figure 7: Flow-focusing channel design for droplet formation

2.4.2   Droplet Sizing

Droplets sizes are determined by a combination of factors. These include: dimensions of microchannels, flow rate of dispersed and continuous phases, and relative viscosity of fluids in both phases as indicated by the capillary number [36]. The influences of these factors on droplet sizes are described in details as follow.

Flow Rate

By decreasing the flow rate of the continuous phase while keeping the flow rate of the dispersed phase fixed, droplet sizes can be increased. Conversely, by increasing the flow rate of the continuous phase while keeping that of the dispersed phase fixed, droplet sizes can be decreased. It is worth noting that increasing the flow rate of the continuous phase not only decreases the size of the droplets but also increases the throughput of droplet formation.

Channel Dimensions

This factor comes into play more in the flow focusing techniques. Generally in the design of flow focusing devices, some degree of roundness is incorporated into the four corners of the flow focusing junction. The radius of roundness of these corners relative to the width of the intersecting dispersed and continuous phase channels has a bearing on the diameter of droplets produced. Gulati et al [39] have shown that the largest droplets are produced in devices where the flow focusing junction corners have the largest rounding, i.e. largest radius of curvature. Also, the size of the orifice of the flow-focusing junction influences the size of droplets produced. The wider the orifices walls, the larger the droplets formed and vice versa. Researchers have demonstrated the size adjustment of droplets by physically varying the dimensions of the orifice using pneumatically controlled walls [40], membrane valves [41].

Capillary Number and Viscosity

Formation of droplets is influenced by a dimensionless factor called capillary number (Ca) [42]. Capillary number is a function of the viscosity of the continuous phase, interfacial tension between the continuous and the dispersed phase, and the velocity of flow of the continuous phase. It is defined by:

$$Ca = \frac{\mu_c v}{\gamma_c}$$

μ_c = viscosity of the continuous phase

v = flow velocity of the continuous phase

γ_c = interfacial tension between the continuous and the dispersed phase

The capillary number determines the droplet break off characteristic of droplets. As previously explained, droplets are formed when the head of the dispersed phase extends into the junction of an intersecting continuous phase and the shear force of the continuous phase flow pinches it causing a break off. Droplet break off usually occur once a set capillary number is exceeded.

2.4.3 Cell Encapsulation

The microfluidic production of encapsulated cells follows the same set of processes required for the formation of droplets, i.e. a controlled emulsification of an aqueous dispersed phase and an immiscible continuous phase. The only difference is that a cell population is added to the dispersed phase. These cells get naturally trapped within the droplets as they are formed during the emulsification process (see Figure 8).
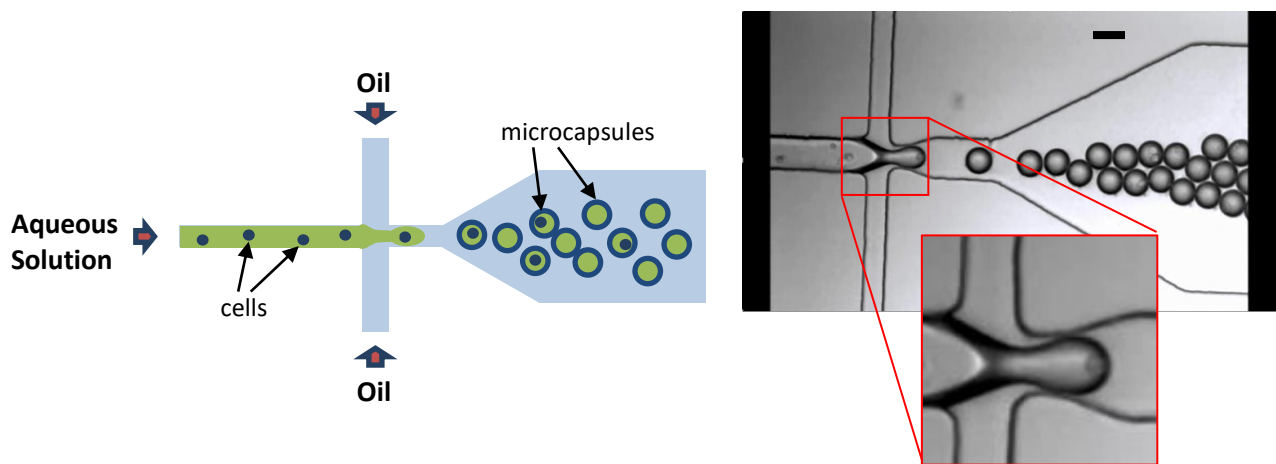
Figure 8: Schematic (left) and Bright Field image (right) of encapsulation of microcapsule through controlled flow focusing of aqueous mixture of cells, media, and agarose. Cells are trapped in droplets formed by the pinching of aqueous flow by transversely flowing oil (scale bar=50µm).

16

In order to provide a suitable semi-permeable extracellular matrix for the cell and also to make the microcapsules structurally rigid, it is usually necessary to add a bio-compatible hydrogel to the dispersed phase. The hydrogel material defines the extracellular environment of the cell as it provides the framework for cell anchorage. The choice of hydrogel material, and consequently extra cellular matrix material, has a bearing on cell viability, function, growth, differentiation, and proliferation [43]. There are several types of hydrogels commonly used for cell encapsulation experiments. The most popular among these are agarose and alginate. These two hydrogels are natural polysaccharide polymers both derived from seaweed extracts [44].

Alginate hydrogel is the more popular choice for cell encapsulation mainly because of its ease of use. However, alginate microcapsules are less stable and less durable, and are more prone to rupturing than deforming under strain [3] [43]. To improve stability and durability of microcapsules, alginate is often coated with poly-L-lysine (PLL). However there are concerns regarding the biocompatibility of Alginate-PLL as PLL exhibits certain levels of cytotoxicity [3] [11].

Agarose on the other hand is a temperature-dependent hydrogel that is rapidly becoming popular in cell encapsulation due to its outstanding mechanical properties. Compared to alginate, agarose has a superior stability and durability [11]. Given these advantages, the hydrogel of choice for the work described in this thesis is Agarose.

The formation of agarose droplets requires a suitable immiscible viscous oil for the continuous phase. A common choice, and also the choice for this project, is mineral oil. Mineral oil is biocompatible and easy to work with on a microfluidic device. Surfactants are typically added to the oil in order to prevent droplets from coalescing [42]. An important requirement for the surfactant is solubility in mineral oil. The commonly used surfactant that fits this criteria is Sorbitan monooleate (SPAN 80).

The next step (see Figure 9) following the formation of droplets in the cell encapsulation process is the gelation of microcapsules. Gelation refers to the cross-linking of networks of polymer chains in the hydrogel to improve its mechanical strength [45]. Gelation is usually triggered by adding an agent, depending on the type of hydrogel. For instance, alginate can be gelled by using an ionic agent, typically by adding a divalent cation such as calcium, barium, or strontium [11]. Whereas agarose is gelled by using a thermal agent, simply by cooling down its temperature. Emulsification of agarose is usually carried out with the agarose in its liquid state typically at about 37°C, and to gel the microcapsules, they are cooled down below room temperature, as low as 17.5°C [46]. Agarose exhibits thermal hysteresis

whereby once gelled, it takes a significantly higher temperature to convert it back to liquid state, typically well above 50°C.

After the gelation step, the next step is to purify the sample by removing the continuous phase oil that is carried over from the emulsification step. Removal of oil is important because oil is an unsuitable medium for long term cell survival. It is necessary to re-suspend the cell-laden microcapsules in an aqueous medium that contains the kind of nutrients and ions needed to maintain regular cell functions, and thus preserve viability [47].
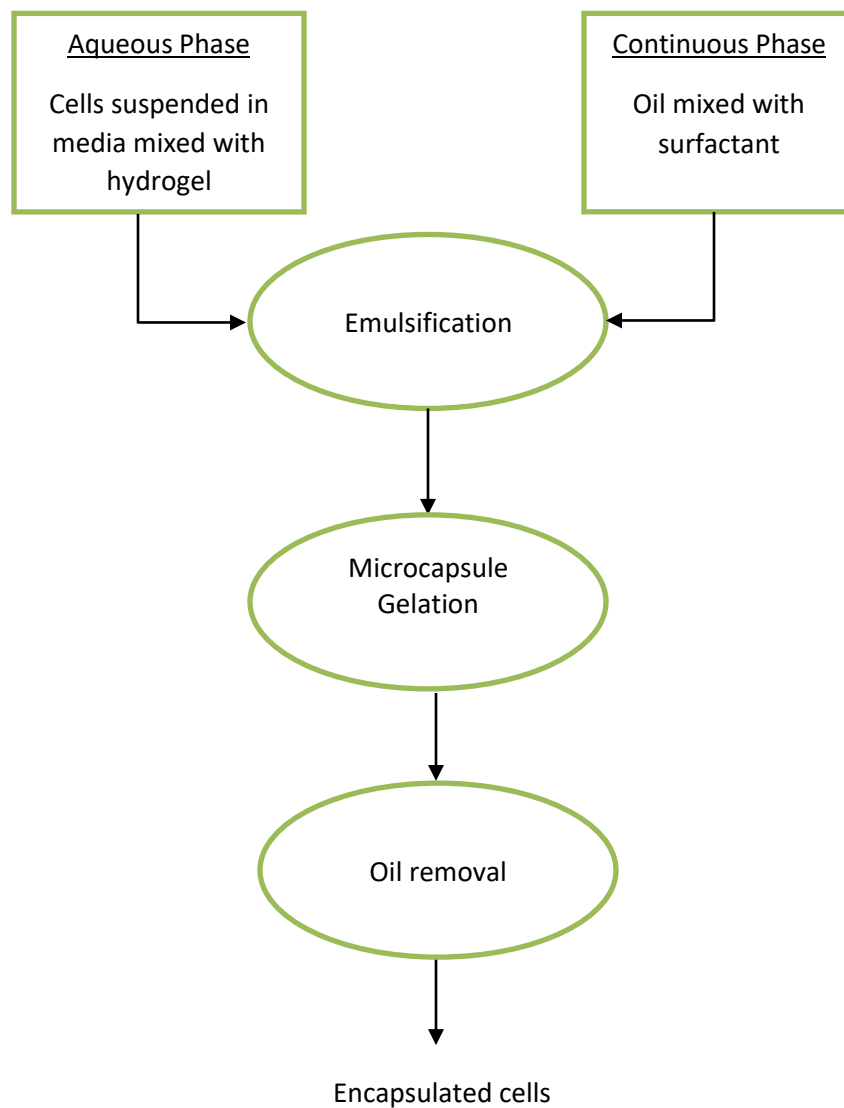
Figure 9: Steps involved in microfluidic cell encapsulation

Removal of oil can be achieved either on-chip or off-chip. There are several on-chip techniques that have been proposed for post-encapsulation removal of oil. Deng et al [47] have demonstrated a microfluidic technique for transferring microcapsules suspended in an oil phase into an aqueous solution using cross flow. Monette-Catafard [46] has also demonstrated the transfer of microcapsules from an oil phase by injecting an aqueous solution at high flow rates in order to displace microcapsules. Nonetheless, off-chip oil removal techniques is still a viable option. This often involves centrifuging the sample (i.e. microcapsules in an oil phase). Since oil has a lower density, it will settle above the microcapsules after centrifugation, and can easily be aspirated. An aqueous cell-culturing media can then be added and the microcapsules resuspended.

2.4.4   Low Conductivity Media (LCM)

After cell encapsulation has been performed, the microcapsule samples collected are usually suspended in a medium favourable for cell subsistence, typically a cell culturing medium. Cell culturing media are aqueous isotonic solutions that are highly rich in free ions which are meant to provide electrolyte balance between the interior of cells and their surrounding environment. While an ion-rich medium is good at maintaining an ionic homeostasis for cells, exposing such medium and the cells it contain to a high electric field environment, as is sometimes the case with DEP and EP, causes a variety of problems that are detrimental to the viability of the cells [48]. In fact, for the DEP experiments described in this thesis, voltages of up to 70V were applied across an electrode spacing of 100μm yielding an effective field strength of up to 700 kV/m. Similarly, for EP manipulations, voltages of up to 1000V were applied across an electrode spacing of 1cm, yielding an effective field strength of 100 kV/m. Subjecting cells to these magnitudes of electric field in a highly conductive ionic buffer medium have been shown to cause cell lysis and cell death [49]. Also, an ion-rich medium promotes galvanic corrosion of electrodes by acting as an electrolyte and facilitating a reduction-oxidation reaction within the microchannel. Furthermore, a highly conductive medium would cause leakage currents within microchannels, which minimizes electric field strength and corresponding DEP and EP forces. Also, high conductive buffers are known to induce Joule Heating within microchannels, causing an increase in temperature [50] [51]. To overcome these drawbacks, an aqueous media that is low in ion concentration, and consequently possess a low conductivity, is often preferred for DEP and EP experiments.

Low conductivity media (LCM) come in different forms and compositions. Their primary requirement is to have a low ion concentration while still able to promote cell viability. There are various LCM that have been proposed over the years. However many researchers tend to gravitate towards sucrose buffers containing 8.5% sucrose and 0.3% dextrose for DEP experiments [52] [53] [54]. This composition has been shown to maintain cell viability for an extended period of time [55].

Chapter 3

DIELECTROPHORESIS CHARACTERIZATION OF MICROCAPSULES

3.1 Theory of DEP Characterization using Hydrodynamic Force

As described earlier in chapter 2, a particle subjected to a non-uniform alternating current (AC) electric field will experience a DEP force, the magnitude of which will vary based on the frequency of the applied AC signal among other factors such as surrounding medium, size and composition of the particle, and the magnitude of the electric field. In other words, DEP is frequency dependent.

DEP force is not a quantity that can be easily measured directly. Hence we need to find a way to translate DEP force into a measurable parameter. Some studies have attempted to quantify DEP force on cells using other means such as levitation [30] or deflection in micro wells [29]. In this chapter, a DEP quantification technique using hydrodynamic force is proposed.

The proposed quantification of DEP force using hydrodynamic force follows Newton's third law of motion: action and reaction are equal and in opposite direction. In our case, the acting force is DEP and the reacting force is the result of hydrodynamic drag (Figure 10). A strong enough DEP force acting on a particle can be used to trap and fix the particle within a fluidic channel. Then a hydrodynamic force, due to flow, is imposed until the particle is displaced. The hydrodynamic drag force at which the particle is released will be equal to the component of DEP force acting along the direction of flow. That is:

$$F_{DEP(x)} = F_{Drag}$$

(11)

By repeating this sequence of DEP trapping and hydrodynamic releasing of particle for varying frequencies over a bandwidth of AC signal and noting the flow pressure at the point of release, we can extract the frequency-dependent DEP characteristic of the particle.

The only drawback to this method is that it is only useful for characterizing positive DEP since it requires particles to be attracted to an electrode in order to be trapped.
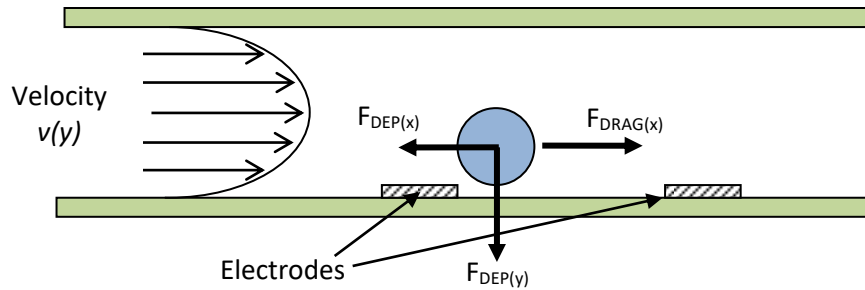
Figure 10: Side view of channel showing DEP and Drag forces acting on a microcapsule

Stokes' equation can be used to find the approximate hydrodynamic drag force acting on the microcapsule, provided that Reynold's Number remains low and flow is laminar. Stokes' hydrodynamic drag force [28] is given as:

$$F_{Drag} = 6\pi\mu r v$$

(12)

μ = coefficient of viscosity (kg/m/s)

r = radius of microcapsule (m)

v = velocity of flow (m/s)

For a pressure-driven fluidic channel with a rectangular cross section of known dimensions, velocity of flow can be determined from the applied pressure using the following equation [56]:

$$v_z = \frac{\Delta P \, h^2}{8\mu l}\left(1 - \frac{4y^2}{h^2}\right)$$

(13)

ΔP = net flow pressure (N/m)

y = distance from center of channel

h = channel height (m)

μ = coefficient of viscosity (kg/m/s)

l = channel length (m)

Given that the velocity profile in a rectangular fluidic channel consists of two components (horizontal and vertical) as shown in Figure 11, the average flow velocity acting on a microcapsule at any particular location along the cross section of the channel is derived from the integral of the velocity function (equation 13) over the cross sectional area of the microcapsule as shown in equations 14 & 15.

(a) Horizontal velocity profile (*v(x)*)

(b) Vertical velocity profile (*v(y)*)

(c) Combined velocity profile (*v(x,y)*)
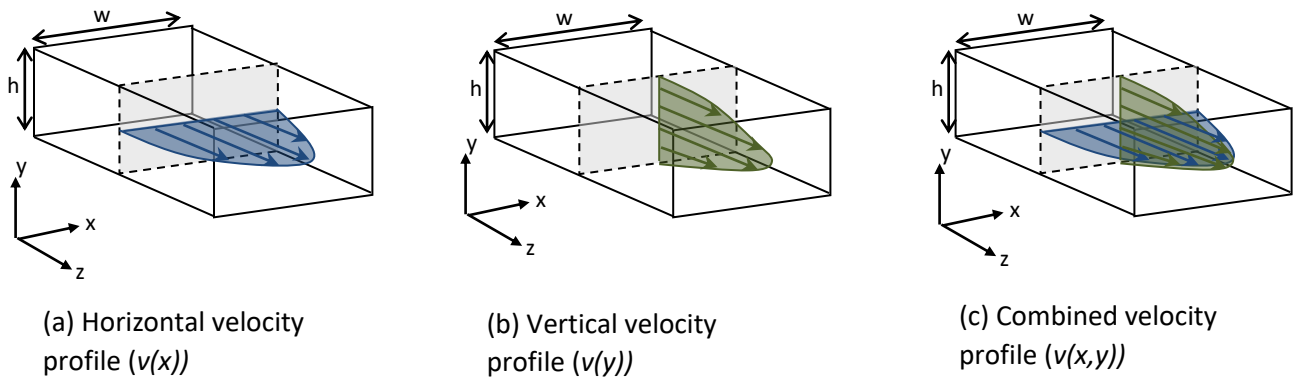
Figure 11: Velocity profiles of flow in a rectangular channel

The limits of the integral assume that the microcapsule is in contact with the floor of the channel and located at the center of the channel width (Figure 12). The integral function (equation 15) assumes that the height of the channel is much smaller than the width, i.e. h/w << 1, thus the velocity is assumed to be constant across the width of the channel. [56].
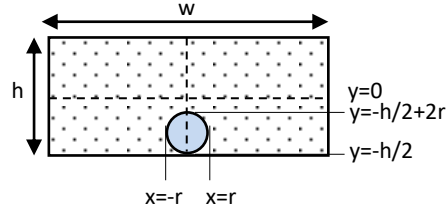
Figure 12: x,y limits for velocity integral of cross-sectional area of microcapsule

$$v_{z(avg)} = \frac{1}{A} \int_A v_z \, dA$$

(14)

$$v_{z(avg)} = \frac{1}{\pi r^2} \int_{-h/2}^{\left(-\frac{h}{2}+2r\right)} \int_{-r}^{r} \left(\frac{\Delta P \, h^2}{8\mu l} \left(1 - \frac{4y^2}{h^2} \right) \right) dx \, dy$$

(15)

3.2   Device Design and Fabrication

There are several techniques of fabricating microfluidic devices such as soft lithography, micromachining, and injection moulding [57]. For this research, soft lithography was the technique of choice. Soft lithography allows for moulding 3-D micro channels in a transparent polymer called polydimethylsiloxane (PDMS) and bonding onto a bottom glass plate, and in our case, one that has been patterned with 50nm thick planar gold electrodes. The proposed microfluidic device for DEP quantification is shown in Figure 13. The design and fabrication process is divided into five stages: channel design, electrode design, electrode fabrication, PDMS mould fabrication, device fabrication/assembly. Each of these steps are described in details. The principle of microchannel design geometry/dimensions as well electrode geometry/dimensions were governed by various factors that are explained in the succeeding sections.

3.2.1 Channel Design

The proposed fluidic channel design is shown in Figure 13. The design was drawn using a CAD program named CleWin. The design consists of two narrow parallel serpentine flow channels that are bridged half-way by a much wider bridge channel. The bridge channel is where hydrodynamic measurement of DEP takes place. At the upstream ends of the serpentine channels are two inlets for the introduction of microcapsules and low conductivity buffer solution into the device, and at the downstream ends are two outlets for the collection of waste microcapsules and buffer solution. The serpentines were designed to be 100um wide to comfortably accommodate a stream of 50-60um diameter microcapsules. The reason for having serpentines as opposed to a simple straight channel is explained later on in the next page. The bridge channel was designed to be much wider than the parallel side channels at 600um in order to slow down the flow velocity in the measurement region for ease of characterization. The length of the bridge channel was set at a reasonable arbitrary value of 5.5mm and has a negligible impact on the characterization procedure.
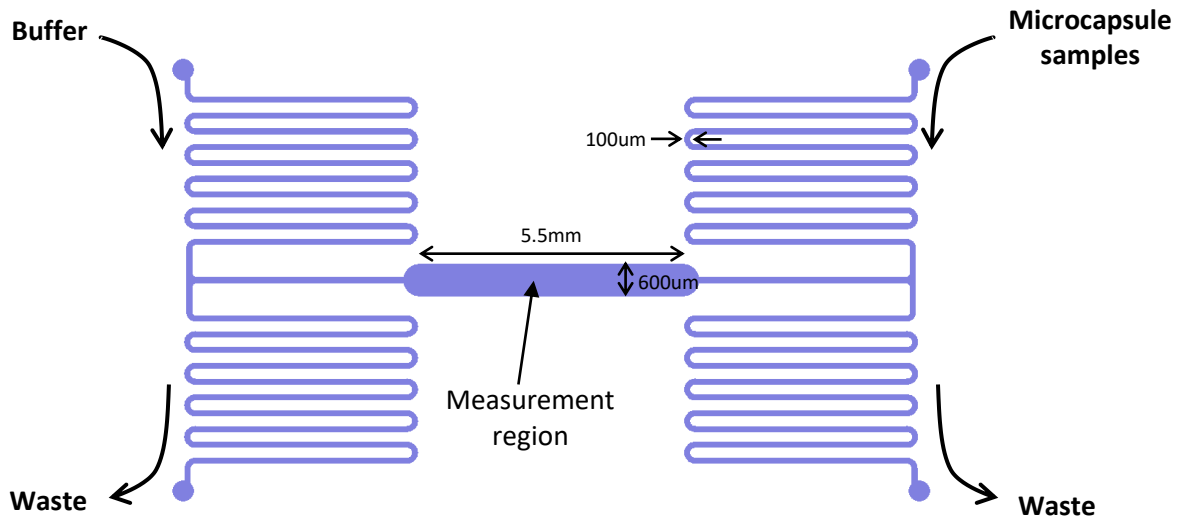
Figure 13: Fluidic channel layout of proposed microfluidic device for DEP characterization

The overall 'H' geometry of the channel was implemented to allow for selective control of the flow of microcapsules into and out the measurement region. By fixing the inlets at a higher pressure compared to the outlets and by increasing or decreasing the pressure of one outlet relative to the other, we can

control the direction of flow into the measurement region - leftward to introduce microcapsule samples for DEP trapping and rightward to introduce buffer solution for hydrodynamic quantification of DEP force.

An illustration of flow control is shown in Figure 14. For the three cases depicted, inlet pressures P_{sample} and P_{buffer} are set to the same value, i.e. $P_{sample} = P_{buffer}$; outlet pressures P_{waste1} and P_{waste2} are set lower than inlets causing flow to always be in the downward direction. If pressure P_{waste1} is set equal to P_{waste2}, net flow in the measurement region will be zero (Figure 14a). If $P_{waste1} < P_{waste2}$, net flow in the measurement region will be leftward (Figure 14b). If $P_{waste1} > P_{waste2}$, net flow in the measurement region will be rightward (Figure 14c).

(a) $P_{waste1} = P_{waste2}$ for zero flow in bridge channel   **(b) $P_{waste1} < P_{waste2}$ for introduction of microcapsule samples to be trapped**   **(c) $P_{waste1} > P_{waste2}$ for introduction of buffer to displace trapped samples**
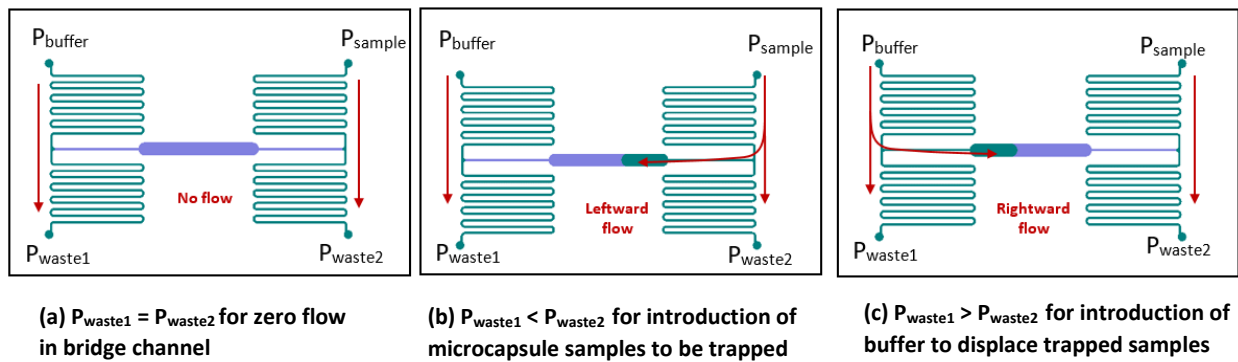
Figure 14: Illustration flow control in the bridge channel by adjusting respective pressure regulators to introduce sample for trapping and to dislodge trapped samples with a buffer solution

An initial design was investigated leading up to the final design described in Figure 13 and Figure 14. The first generation design shown in Figure 15 follows the same operational principle as the final design. The design was functional but had one major limitation in that flow through the measurement region was highly jittery when zero flow condition is applied. It was this limitation that prompted the introduction of serpentines into the stems of the 'H' geometry in the final design to add some flow resistance in the side channels. The increased flow resistance in the side channels results in the flow rate being less sensitive to small fluctuations in pressure which allows for a better zero-flow stability in the measurement channel.
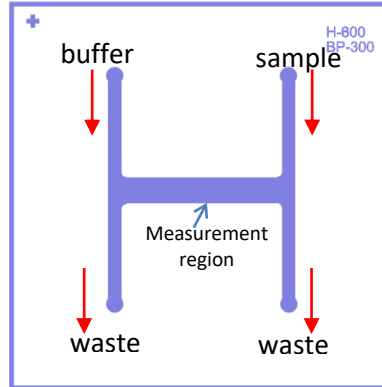
Figure 15: First generation channel design for hydrodynamic DEP quantification. This design made it challenging to create a stabilized flow in the bridge channel due to the shortness of the side channel which creates a very low flow resistance in the side channels and causing the bridge channel to be prone to jitters.

3.2.2 Electrode Design

As described earlier, DEP force on microcapsules will vary based on the physical dimensions of the capsule, dielectric properties of the material that the capsule is composed of, and very importantly, the magnitude and frequency of the applied electric field. In order to maximise the DEP force that acts on the capsule, it is important to design electrodes in a way that maximizes electric field gradient. An optimally designed electrode will not only provide stronger electric field gradient but will do that at lower voltages.

The first generation design consisted of two parallel rectangular arrays running across the width of the channel in the measurement region as shown in Figure 16a. This design, upon testing, worked effectively at trapping microcapsules near the edges of the electrode, where the electric field gradient is largest. However, it does introduce a certain complexity into potential use for hydrodynamic measurement of DEP force. This is because microcapsules are trapped at random locations in the region of electric field between the electrodes. From previous discussions in section 2.1.2, it was shown that hydrodynamic drag force in a pressurized channel varies across channel width, being maximum at the center and decreasing towards the edges. Therefore a microcapsule trapped close to the edge will require higher flow pressure to overcome DEP force than one located in the center. Consequently, hydrodynamic forces have to be normalised for each measurement, taking into account the exact location of microcapsule along channel width.
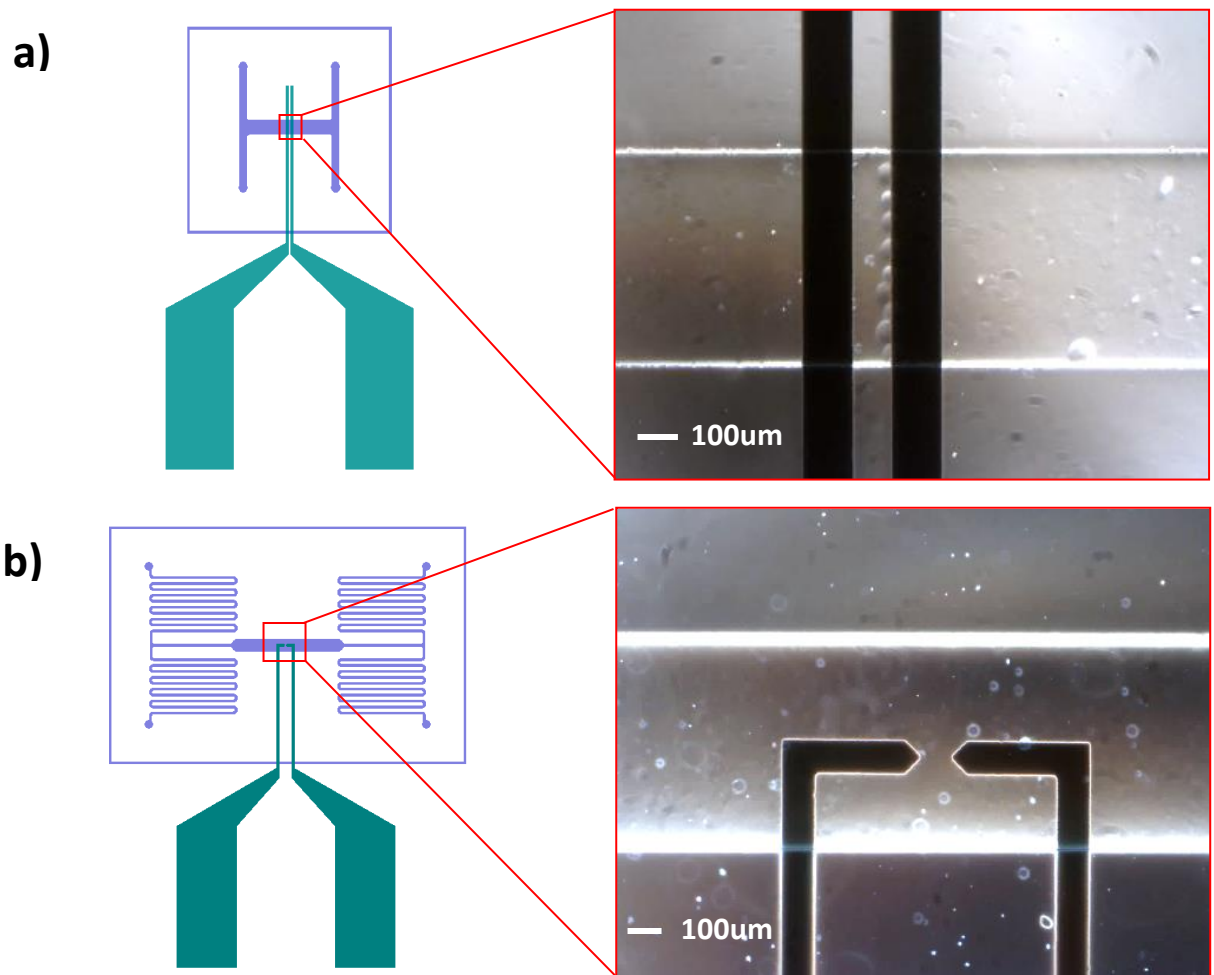
Figure 16: Electrode designs (a) first generation design [electrode width = 150µm, spacing between electrodes = 100µm, channel width = 600µm]; (b) second generation design [electrode width = 100µm, spacing between electrode tips = 100µm, channel width = 600µm]

One way around this limitation is to create a design that concentrates electric field at a fixed location across the channel width. This way, microcapsules are consistently trapped in the same location for each measurement, making it easier to compare results obtained from the trapping of different microcapsules. Our second generation design addresses this. The second generation design (Figure 16b) consists of a pair of triangular-tipped electrodes facing each other, positioned at the center of the channel.

In order to verify the electric field pattern produced by the second generation electrode geometry, a simulation was performed using COMSOL Multiphysics® modelling software. Figure 17 shows the results of a 2D COMSOL rendering of electric field produced by the triangular-tipped electrodes for an applied voltage of 70V. For the simulation, the electrode properties were defined as solid gold metal while the surrounding space were defined as a low conductive liquid (conductivity = 10mS/m). Results confirmed

that electric field is indeed concentrated at the tips of the electrode and gradually disperses as we move away from the tips. This is illustrated by the dark red colour grading at the tips which indicates a high electric field strength. Upon repeated laboratory testing, this design was also found to produce stronger DEP force at a much lower voltages compared to the first generation design.
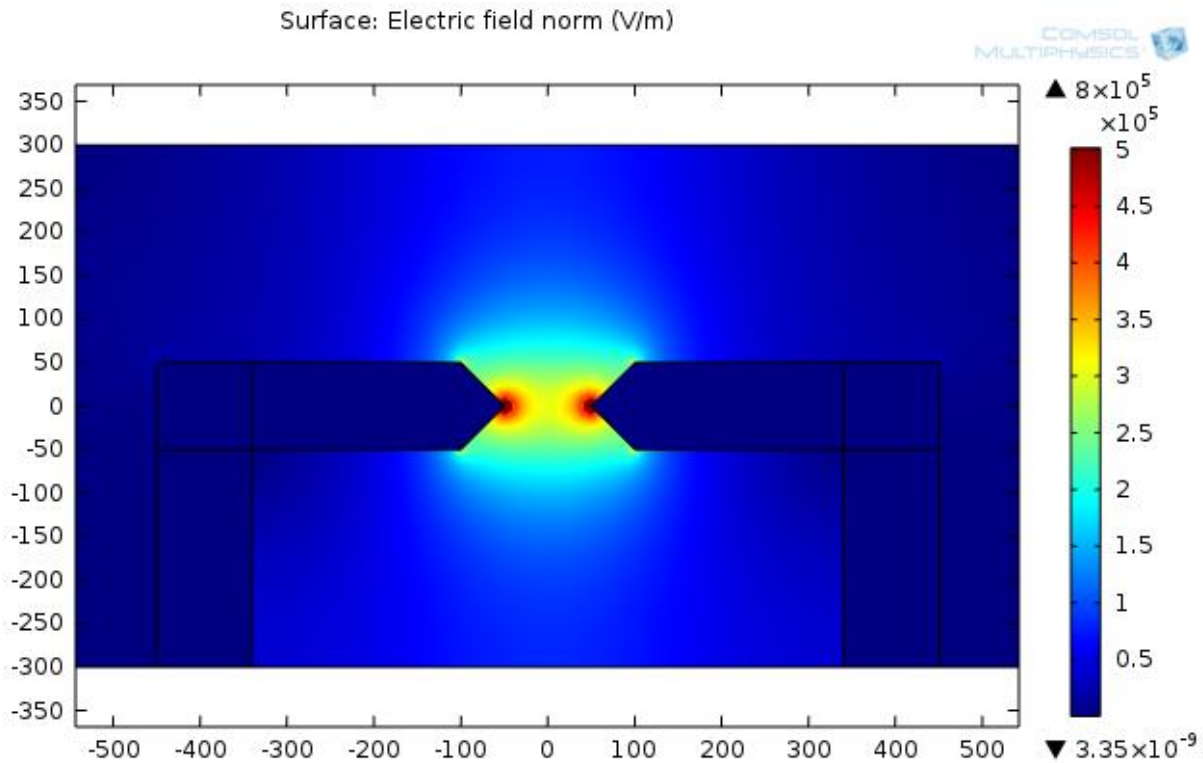
Figure 17: Electric field simulation for the second generation electrode design featuring triangular tips. Simulation was performed using COMSOL® Multiphysics software [electrode width = 150µm, spacing between electrode tips = 100µm, channel width = 600µm]

3.2.3 Electrode Fabrication

Planar gold electrodes on glass substrates were adopted for our DEP experiments. Planar electrodes are advantageous in simplifying their integration into fluidic microchannel as they can be fabricated at heights of tens of nanometer and pose negligible obstruction to flow in micro channels. They also inherently yield regions of high electric field gradients.

Designs for the electrode were drawn using the CAD program CleWin4 and were sent out to a commercial printing service for high resolution printing on positive polarity photomasks.

29

The fabrication of planar electrodes begins with metal deposition on a glass slide. Glass slides (VWR microscope slides 75x25x1 mm) were cleaned and sent off to a deposition facility at Carleton University in Ottawa, Canada, where they were coated with 5nm chromium adhesion layer followed by 50nm gold layer. When the coated glass slides arrived, they were then patterned using a photolithography approach tailored for glass substrates. Full photolithography protocols are attached in the appendix. Briefly, the gold plated glass slides were coated with photoresist (S1813), spun using a spin-coater at 1000 rpm for 30 seconds, pre-baked at 115°C for 80 seconds, exposed to ultraviolet light through masks at 30 watts for 10 seconds, post-baked at 115°C for 80 seconds, and developed for 45 seconds using 10% tetramethylammonium hydroxide (TMAH) solution. To remove unwanted gold and chromium in blank regions of glass side outside of electrodes area, wet etching was performed. First, the unwanted gold layer was etched by dipping in 50% Aqua Regia solution (1 part HNO_3 + 3 parts HCl + 4 parts H_2O) for approximately 15 seconds. This removes unwanted gold but exposes the chromium adhesion layer beneath. The unwanted chromium layer was etched using commercially sold chromium etchant (Model: Transene Chromium Etchant 1020AC) by dipping in the etchant solution for 45 seconds to 60 seconds until the characteristic dark tint of chromium completely faded from the glass slide. Final step was to dip the glass slides in 1165 photoresist developer solution for about two minutes to remove the cured photoresist layer covering the electrode regions.

3.2.4 Master Mould Fabrication

As earlier discussed, fluidic channels are formed in PDMS – a transparent and biocompatible polymer. However in order to cast the microchannels in PDMS, a mould carrying the designs of fluidic channels has to be fabricated first. Moulds are typically made on silicon wafers using soft-lithography techniques.

For our DEP devices, channel designs were drawn using CleWin4 software. Just as in the electrode designs, microchannel designs were sent to a commercial photomask printing service for high resolution printing on negative polarity photomasks.

Fabrication steps begin with acetone and ethanol cleaning of the silicon wafer, followed by spin-coating of SU-8 photoresist at a spin velocity tailored for the desired height of microchannel. Channel height is defined by the achieved thickness of photoresist on wafer surface post-spinning. Immediately after spinning, the SU-8 photoresist layer is cured by soft baking the wafer on a hot plate for a duration pre-determined given the target thickness of the SU-8 photoresist layer. The baked wafer is allowed to cool

down to room temperature and then exposed to UV light through the filter of photomasks carrying fluidic channel designs. UV exposure duration is tailored for the thickness of photoresist. Following UV exposure is another baking process on hot plate, this time to accelerate the polymerization SU-8 photoresist. Afterwards, the wafer is allowed to cool down to room temperature, and then dipped in a developer solution for development. The wafer is rinsed with isopropanol and then hard baked at 150°C for ten minutes. A detailed protocol of the soft-lithography process and parameters used is provided in the appendix.

3.2.5 Device Assembly

The master mould allows for multiple PDMS replications of fluidic microchannel layouts of individual devices. Imprints of microchannels are formed on PDMS by pouring liquid PDMS mixed with crosslinking agent over the master mould and allowed to cure in an oven at about 70°C for about two hours. Once the PDMS is cured and fully hardened, it is peeled off the master mould. The peeled PDMS carries with it replicas of microchannel designs contained on the master mould. It is then cut into blocks, each block containing designs for a single device. The PDMS blocks are then perforated with 0.75mm diameter holes into which tubing are inserted in order to deliver fluids and samples to the microchannels and to collect end-products and wastes. Afterwards, the PDMS blocks together with the glass substrate mentioned in section 3.2.3 containing patterned electrodes are plasma treated. Plasma treatment promotes permanent bonding of PDMS to glass through the exchange of oxygen radicals. The PDMS block and the glass substrate are aligned using an aligner so that the electrodes line up perfectly at their intended locations within the microchannel. The two entities are then pressed together to form a permeant seal. Figure 18 shows a photograph of a completely assembled DEP characterization device.
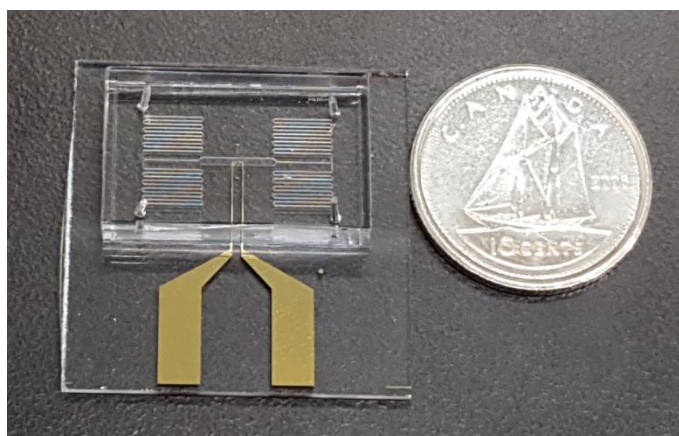
Figure 18: Picture of fully assembled DEP characterization device next to a 10 Canadian cents coin

3.3   Cell Culturing

The cell line used for this study is NIH 3T3 mouse embryonic fibroblast cells. This is an immortalized stem cell developed in 1962 by George Todaro and Howard Green of New York University School of Medicine [58]. One of its defining characteristics is fast growth rate with cell populations essentially doubling approximately every 24 hours. The 3T3 cells used for experiments presented herein were cultured in 100mm diameter petri dishes using Dulbecco's Modified Eagle Medium (DMEM) with added supplements of 10% fetal bovine serum (FBS) and 1% penicillin-streptomycin (PS), and kept incubated at the temperature of 37°C and CO_2 level of 5%. Characteristically, cultured cells attach to the bottom of the petri dishes they are held in, hence for splitting or harvesting purposes, have to be detached using trypsin.

After having grown to about 80 percent confluency, cells were trypsinized using 0.5% trypsin and collected in a falcon tube. Collected cells in trypsin were supplemented with DMEM, counted by hemocytometer, and centrifuged at 1000 revolutions per minute for three minutes after which supernatant solution was aspirated and cell pellet re-suspended in low conductivity media consisting of 8.5% sucrose and 0.3% dextrose in H_2O ready for experimentation.

3.4   Cell Encapsulation Method

The encapsulation of cells was done using the microfluidic device shown in Figure 19. The device was developed by a previous graduate student of The Godin Lab at University of Ottawa, Nicolas Monette-Catafard, for his Master's Thesis [46]. The device is able to generate droplets through controlled emulsification of aqueous agarose cell mixture and oil.
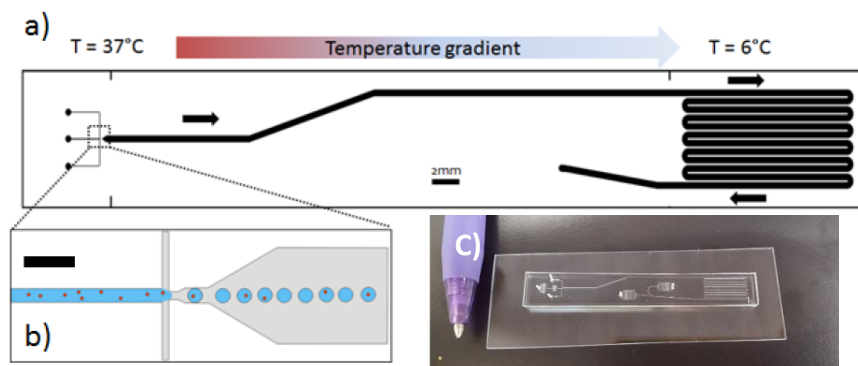
Figure 19: Microfluidic device for cell encapsulation ©Nicolas Monette-Catafard 2014. (a) Microfluidic device; (b) encapsulation illustration; (c) photo of completely assembled device

The encapsulation process begins with the preparation of agarose gel, followed by mounting of the encapsulation device into the temperature controlled block shown in Figure 20. Temperature of the heating block is set at 37°C – the most optimal temperature for maintaining cell viability. Temperature of the cooling block is set to 4°C to expedite the gelation of agarose without causing much harm to the cells. Next, the cells to be encapsulated are harvested in low conductivity media following the steps described in section 3.3. The cells are then mixed with agarose solution at 37°C to achieve cell concentration of about 10 million per ml, and agarose concentration of 2%. The mixture is fed into the aqueous inlet of the encapsulation device while mineral oil (Sigma-M904) with 1.5% surfactant (SPAN) is fed into the oil inlets. All inlets are then pressurised to drive the cell mixture and oil into the device for microcapsule formation. The finished product, gelled microcapsules are collected in low conductivity media ready for DEP experimentation.
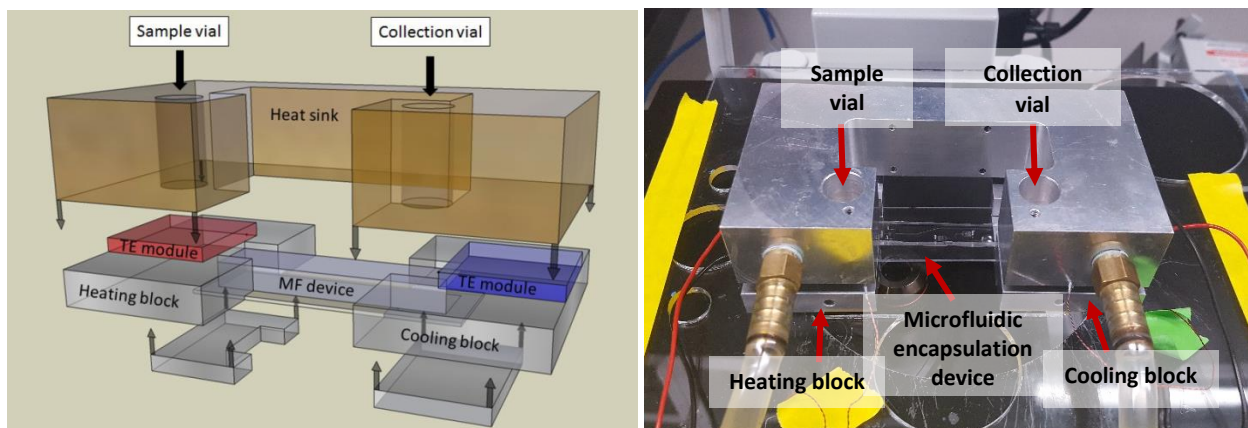
Figure 20: (a) Schematic of temperature control block for cell encapsulation. The block consists of a heating module that keeps cell sample warm at 37 degrees Celsius, and a cooling module for the gelation of agarose capsules at 4 degrees Celsius ©Nicolas Monette-Catafard, 2014 (b) Photograph of the temperature control block.

3.5   Experiment Setup

A block diagram of the experiment setup is shown in Figure 21. It comprises of three stages: capture, pneumatic, and electrical. The capture stage consists of a microscope (Model: Olympus IX51) fitted with a 4X objective (Model: Olympus UPlanfl 4x/0.13 PHL ∞/-) and a camera with a capture rate of up to 60 FPS (Model: PointGrey BFLY-PGE-13E4C-CS). The camera is connected to a PC via a gigabit ethernet interface. Images and videos from the camera are captured on the PC using the PointGrey FLyCapture

software. The camera was used to monitor flow of microcapsules and buffer solution into the measurement region of the channel in order to capture and record microcapsule activities pertaining to DEP trapping and hydrodynamic displacement.

The pneumatic stage consists of three pressure regulators (Model: 2xBellofram regulator type 10; 1xSMC ITV1011) controlling fluidic access to the device. The regulators are connected in the configuration shown in Figure 22. Given that both inlets of the device have to operate at equal pressures, it was considered ideal to couple them to a singular pressure output using a tee connector. That way, both inlets take up just one pressure regulator and are certain to be under equal pressure. The outlets on the other hand were regulated separately; one regulator connected to waste outlet 1 and another connected waste outlet 2.

The electrical stage consists of a function generator (Model: Tektronix AFG 2021), a radio frequency power amplifier (Model: OPHIR 5048), and an oscilloscope (Model: Agilent DSO1014A). The function generator was rated for maximum AC voltage of 10 V peak-to-peak and maximum frequency of 20 MHz. Because the 10 V maximum output of the function generator is too low for the intended DEP application which can require upwards of 70V, there was need for it to be connect to a power amplifier that is rated for high power and high bandwidth. The only RF amplifier available for use for the project has an operational bandwidth of 150 kHz to 230 MHz. This unfortunately meant that frequencies below 150 kHz could not be examined during our DEP quantification experiments using the available RF amplifier. The output of the RF amplifier was split two ways using a BNC tee connector: one line connected to the oscilloscope for monitoring, the second line connected to the electrodes on the microfluidic device. One end of the electrode acted as reference (or ground) lead while the other end acted as signal lead. The BNC connection to the device was impedance-matched using a 50 ohm RF rated resistor to prevent signal reflections back into the amplifier – a prominent phenomenon that occurs at high frequencies and compromises the integrity of AC signals. The planar gold electrode pads on the glass substrate of the device were connected in parallel to the impedance matching resistor using a high conductivity silver epoxy solder.
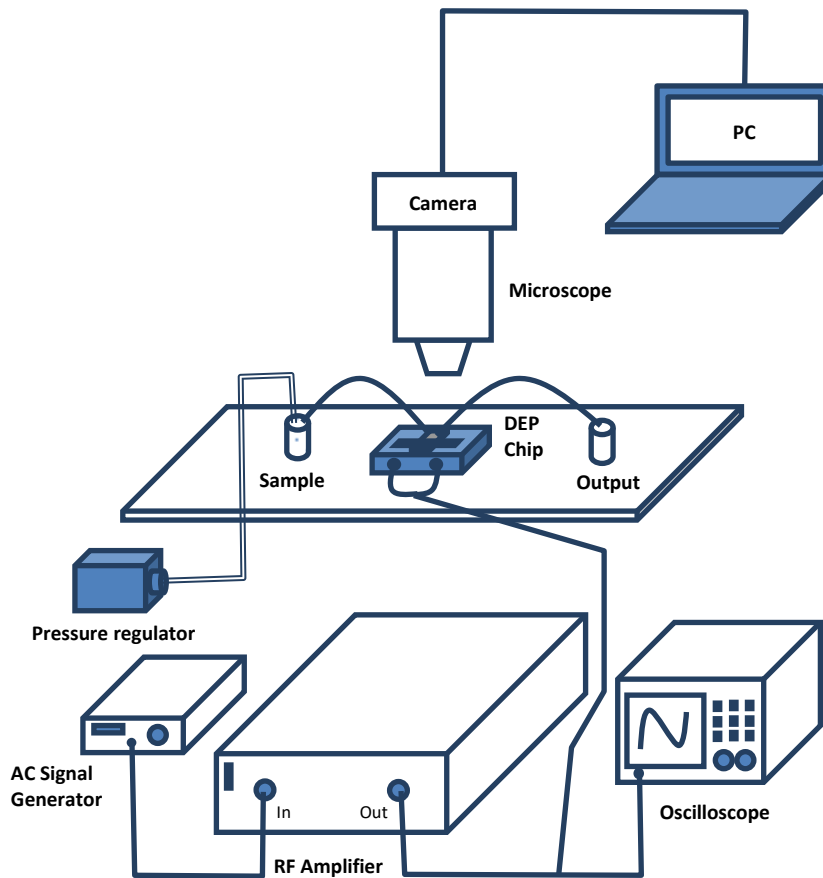
Figure 21: Schematic of equipment setup used for running dep experiments

3.6   DEP Characterization Method

For the DEP characterization experiments, microcapsule samples were injected into the device (see Figure 22) through the top right inlet while a low conductivity media containing 8.5% sucrose and 0.3% dextrose was injected through the top left inlet. The two inlets were connected to one pressure regulator. Pressure P1 was maintained at 10 psi during experimentation. The two outlets were connected to separate pressure regulators P2 and P3. Pressure P3 was maintained at 7.5 psi while P2 was varied to control the direction and velocity of flow in the bridge channel. When P2 = P3 = 7.5 psi, there is zero flow in the bridge channel; when 7.5 psi < P2 < P1, flow in bridge channel is in the rightward direction; when P2 < 7.5 psi < P1, flow in bridge channel is in leftward direction.
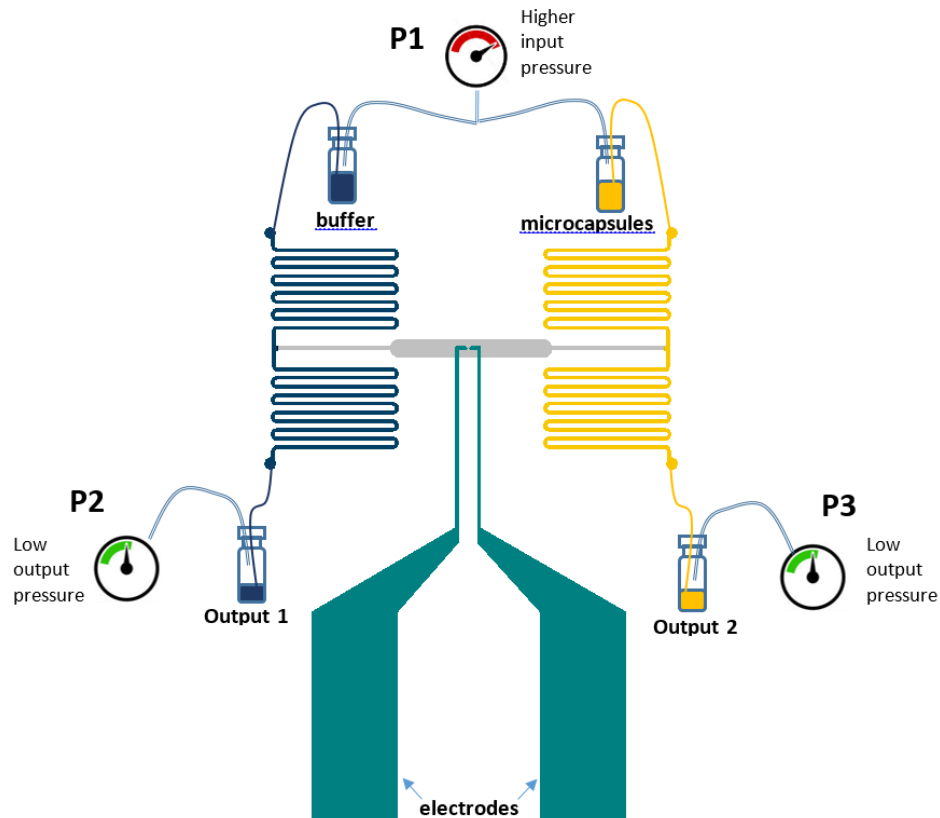
Figure 22: Illustration of fluid control in the device using a combination of three pressure regulators

Microcapsule are introduced into the bridge channel by setting P2 < 7.5 psi. Once there are microcapsules in the vicinity of the electrode tips, the flow in the bridge channel is stalled by setting the pressure P2 to approximately 7.5 psi. An electric field is then applied to the electrode at a voltage and frequency known to generate a DEP force strong enough to attract and trap microcapsules at the triangular tip of the electrode. This voltage and frequency, from experience in testing the device, lie anywhere between 40V to 50V and 150 kHz to 2 MHz. Once the electric field is turned on, any microcapsule in the viscinity of the electrode tip is pulled towards the electrode by the DEP force and trapped at the tip (see Figure 23). Once a microcapsule has been trapped, the voltage is then set to 40V and the frequency is set to the value being investigated. Flow of buffer solution is then directed into the bridge channel by gradually increasing pressure P2 while also monitoring the trapped microcapsule. The pressure P2 is continuously increased at a steady rate causing an increase in the flow velocity of buffer solution through the bridge channel, until the microcapsule is swept off its trapped position at the electrode tip. The value of pressure P2 at which microcapsule is displaced is noted down. This pressure

value is then used to calculate the hydrodynamic force exerted on the microcapsule at the moment it was displaced from the electrode tip (using equations 13-15). The calculated hydrodynamic force is equal to the component of DEP force acting on the microcapsule along the direction of flow. The process is repeated for multiple frequency points of the applied AC signal. A graph is the plotted that shows how DEP force varies with frequency.
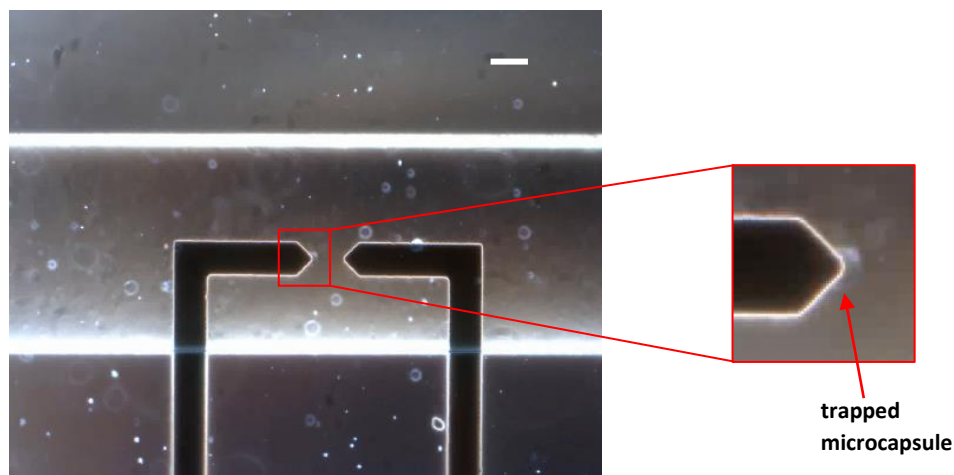
Figure 23: Microscope capture showing a 50µm diameter microcapsule trapped at the electrode tip (scale bar = 100µm)

3.7   Results and Discussion

The goal of the DEP characterization experiments is to determine the DEP properties of empty microcapsules and that of cell laden microcapsules, and then propose an ideal condition for sorting based on the characterization results. Since DEP force varies with frequency, measuring the exact DEP forces exerted on empty and occupied microcapsules over a range of frequencies will give useful pointers as to which frequencies are best for sorting, ideally the ones at which DEP forces on occupied microcapsules differ the most from empty microcapsules.

The frequency-dependent DEP spectra of 2% agarose microcapsules in a low conductivity media (8.5% sucrose + 0.3% dextrose in distilled water) were determined using the hydrodynamic technique described earlier. Results are shown in Figure 24. The microcapsules tested were 50µm in diameter. Two

spectra were obtained, each representing one of the two conditions: no cell in microcapsule (i.e. empty), and single cell in microcapsule (i.e. occupied). Each spectrum is an average of six different experiments. The error bar on each data point represents the standard error of six different measurements, each measurement based on different microcapsules. The voltage of the applied AC signal is fixed at 40V peak-to-peak and frequency is varied from 150 kHz to 7MHz.
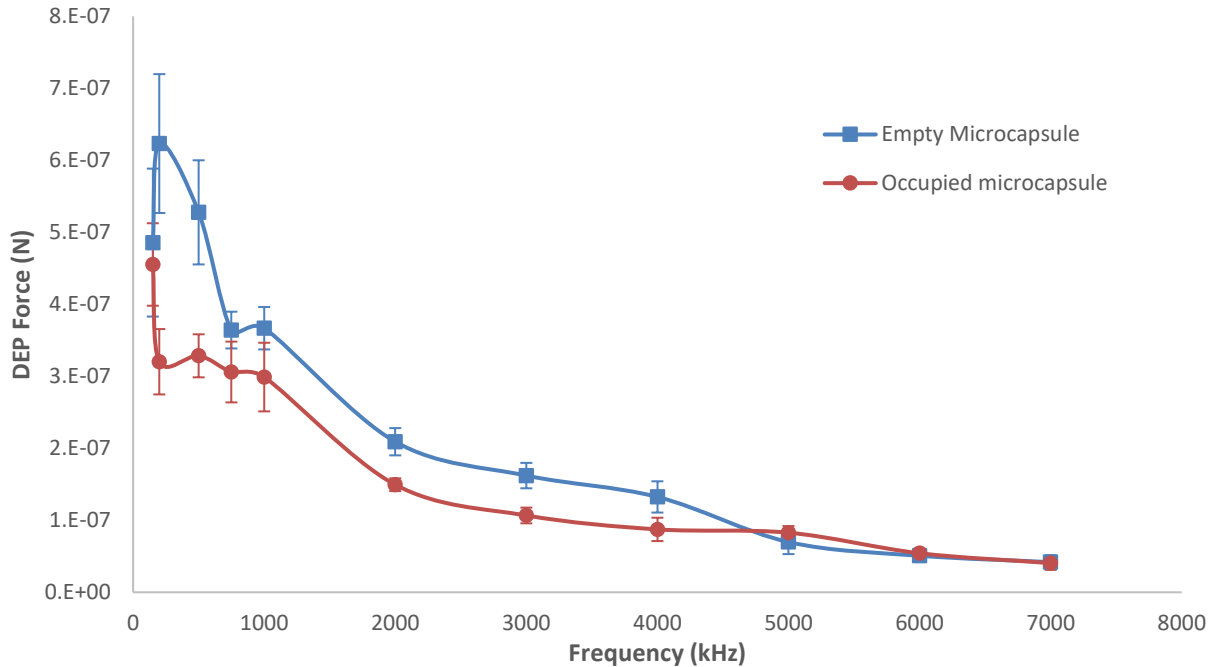
Figure 24: The component of DEP Force acting on microcapsules in opposition to flow versus the frequency of AC signal used to generate the DEP force

As shown in Figure 24, for both empty microcapsules and occupied microcapsules, the DEP force experienced is higher at lower frequencies and gradually diminishes as frequency increases. The stronger DEP forces recorded at lower frequencies implies that it took a stronger hydrodynamic force to displace microcapsules from their trapped position at the tip of the electrode. Conversely, at frequencies higher than 7 MHz, DEP force significantly weakens. Microcapsules after this point barely experience a DEP force strong enough to keep them trapped at the tip, making it impossible to characterize them. However, just to be certain that the weak DEP force beyond 7 MHz is not a mere inherent short-lived drop that later picks up at a higher frequency, we tested frequencies beyond 7 MHz at increments of 1 MHz up to the maximum frequency of 20MHz supported by our function generator.

No interesting observation was made as the weak DEP force persisted all the way from 8 MHz to 20 MHz.

Comparing the spectrum of empty microcapsules to occupied, there is a degree of similarity in the overall trend. However the average DEP force on empty microcapsules is higher in the range of 150 kHz to 4 MHz. From 4 MHz to 7 MHz, both spectra seem to overlap. Frequency limitations in the RF amplifier instrument prevented us from examining the DEP response at frequencies lower than 150 kHz.

This method is not without certain inherent flaws. One of its biggest disadvantages is low sensitivity to weak DEP forces as highlighted by the fact that we could not characterize frequencies where microcapsules could not adhere to the electrode tip. The technique requires that microcapsules be trapped at the tip of the electrode and only a strong enough DEP force can accomplish that. We observed that when the DEP force is very low, microcapsules barely get trapped, they hang loosely around the electrode tip and get released at the slightest increase in flow. Another inherent flaw of this detection technique is that it does not support the characterization of negative DEP forces. As explained in section 2.2, a DEP force is negative when it causes motion away from the electrode. Since this method relies on microcapsules being trapped at the electrode, only positive DEP could be quantified.

Nonetheless, the objective of the quantification experiment of finding a suitable frequency for sorting was achieved. Results showed that DEP sorting could be possible in the range between 150 kHz to 3000 kHz as empty microcapsules experience a notably different DEP force from occupied microcapsules in this range.

Chapter 4

ELECTROPHORESIS CHARACTERIZATION OF MICROCAPSULES

In this chapter, the characterization of the electrophoretic (EP) effect on microcapsules is described. The goal of the EP characterization experiments performed was to establish the differences in EP response between cell-laden microcapsules and empty microcapsules. Knowing this behaviours will provide useful information that can help facilitate sorting.

4.1   Theory of EP Characterization

Electrophoresis, as explained in section 2.3, is a phenomenon that describes the movement of a charged particle through a fluid in the presence of an electric field [28]. A positively charged particle will exhibit motion towards the negative electrode while a negatively charged particle will exhibit motion towards the positive electrode. The net force imposed on the particle is as a result of the balance between electrostatic force and hydrodynamic drag. Initially, upon application of electric field, the particle accelerates. However, the acceleration quickly decreases to zero as electrostatic force equals hydrodynamic drag, causing the particle to move at a constant terminal velocity. The terminal velocity of motion depends on the electrophoretic mobility of the particle which is a function of charge density as shown by the equations 16 and 17 [28]:

$$v_{particle} = \mu_{ep}E$$

(16)

$v_{particle}$ = terminal velocity of particle

μ_{ep} = electrophoretic mobility of particle

E = applied electric field

Electrophoretic mobility (μ_{ep}) is defined as:

$$\mu_{ep} = \frac{q}{6\pi\mu r}$$

<div align="right">(17)</div>

q = particle charge

μ = coefficient of viscosity of buffer solution

r = radius of particle

From equations 16 and 17, the terminal velocity of a particle subjected to an electric field in a viscous fluid is directly proportional to the charge of the particle. That is the higher the particle charge, the higher the terminal velocity of its resulting EP motion. The terminal velocity of microcapsules can be determined by measuring the time required for a microcapsule to travel a set distance in a microchannel under the influence of a uniform electric field. The EP forces acting on a microcapsule can therefore be characterized by plotting the terminal velocities of motion against varying applied electric fields.

4.2   Device Design and Fabrication

4.2.1   Channel Design

The EP characterization device (see Figure 25) consists of a single straight channel 4.5cm long, 400μm wide, and 120μm tall. The design features a fluidic inlet and outlet at the tail ends of the channel. Along the length of the channel are two access points spaced 1cm apart for the insertion of two silver wire electrodes. A voltage difference is then applied between the cathode and the anode. This minimal straight-line channel design suits our quantification objective which is to measure the velocity of microcapsules under the influence of a uniform electric field by measuring the time it takes the microcapsule to travel a set distance in a straight line trajectory.
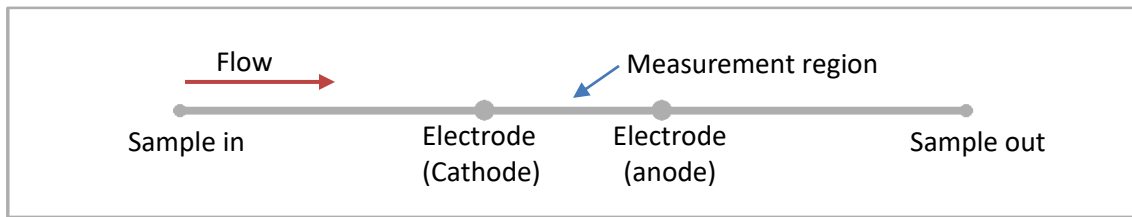
Figure 25: Channel design for EP characterization device

4.2.2 Electrodes

Unlike the DEP quantification device where planar electrodes were patterned on the floor of the microchannel thereby providing a non-uniform electric field that is strongest along the floor of the channel and weakens towards the roof of the channel, the proposed EP quantification method demands an electrode option that provides maximum uniform electric field across the cross section and the length of the channel. A feasible solution for the electrode implementation was to simply insert two wires directly into the channel through a pair of punched PDMS hole (see Figure 26) and connect the opposite ends of the wire to a DC voltage source. The wires are made of thin silver material wrapped in polyethylene sleeve. A tiny segment was left exposed in the end connected to the microchannel for contact with fluid flowing through the channel. The polyethylene sleeve helps to seal the electrode access points to prevent the leakage of fluid flowing through the microchannel.
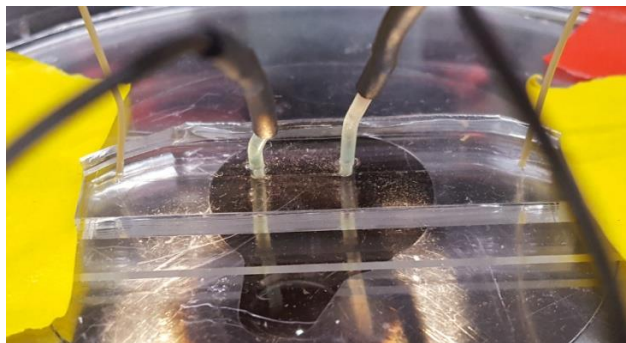
Figure 26: Picture of characterization device showing electrode connection

4.3   Experiment Setup

A block diagram of the electrophoresis characterization setup is shown in Figure 27. Similar to the dielectrophoresis setup presented in section 3.5, this setup comprises three stages: capture, pneumatic, and electrical. The capture stage is exactly the same as that of the dielectrophoresis setup, however the pneumatic stages and the electrical stages have been modified to suit requirements for the new EP microfluidic device and for electrophoresis experiments.
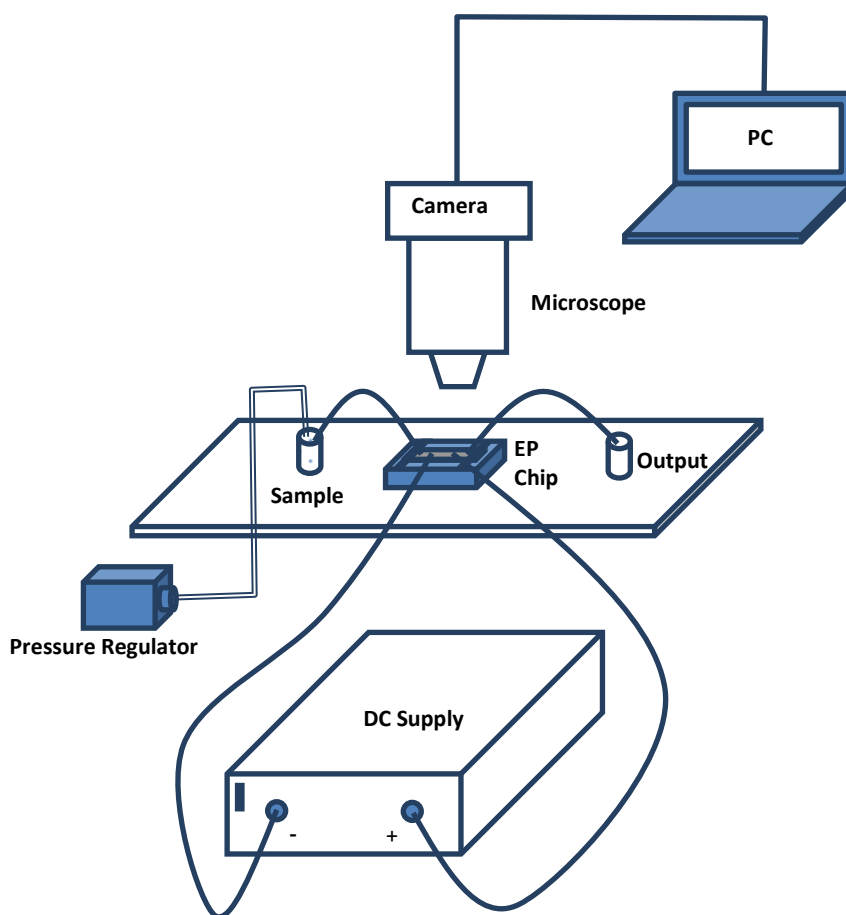
Figure 27: Schematic of equipment setup used for running EP experiments

The pneumatic stage consists of just one pressure regulator that is connected to the inlet vial and controls the supply of samples to the microfluidic device. The outlet is kept at atmospheric pressure. The

electronic module is configured to provide a DC voltage to the microfluidic device. It consists of a DC supply (Model: Keithley 237) capable of producing voltages up to 1100V.

4.4   EP Quantification Method

Firstly, encapsulated cell samples (3T3 mouse fibroblast) were prepared and suspended in low conductivity media (see sections 3.3 respectively for cell preparation and section 2.4 for cell encapsulation methods). The sample vial is connected to the inlet of the EP device via thin PEEK tubing and pressurized to deliver cells or microcapsule samples into the fluidic channel. Once the channel is filled with LCM buffer carrying containing microcapsule samples, the flow is completely stopped by balancing the inlet pressure with the outlet pressure at atmospheric pressure. This was done by disconnecting the inlet pressure regulator from the inlet vial and loosening the caps of both inlet and outlet vials. This technique was found to be the most effective at creating a zero velocity, jitter-free flow in the microchannel.

The next step was to visually select a sample (cell or microcapsule) for measurement, activate video recording on the microscope camera which was set to record at 60fps, apply DC electric field to the device, and capture a video of the sample moving through the channel in response to the electric field. The video is later analyzed to extract velocity of movement of the sample. This was done by going through the video frame-by-frame to measure the time it takes for the microcapsule sample to cover a set distance within the microchannel using ImageJ software.

4.5   Results and Discussion

Experiments were performed with microcapsules suspended in a low conductivity media of distilled water with 8.5% sucrose and 0.3% dextrose. The media has a measured pH of approximately 7. Electric field was applied using electrodes inserted into the PDMS channel and spaced 1cm apart.

Figure 28 shows the results obtained from velocity characterization of empty and cell-laden microcapsules when subjected to varying strengths of electric field. For comparison purpose, non-encapsulated cells were characterized as well. Six experiments were performed for each of the three conditions. In each experiment, a different microcapsule or cell was used. Data points on the graphs

thus represent averages of six different measurements; error bars represents standard error of the six data. Microcapsules were approximately 50µm in diameter.

In all three cases (cells, empty microcapsules, occupied microcapsules), electrophoretic migration was observed in the direction of the anode. This suggests that the net charge of microcapsules (empty or containing cell) as well as cells is negative. The net negative charge observed for cells in this experiment is consistent with many reports in the literature that have shown that most cells are covered with negatively charged functional groups at a neutral pH [59] [60]. Likewise, agarose gel which the microcapsules are made of has been shown to contain certain negatively charged groups such as pyruvate and sulfate [61].
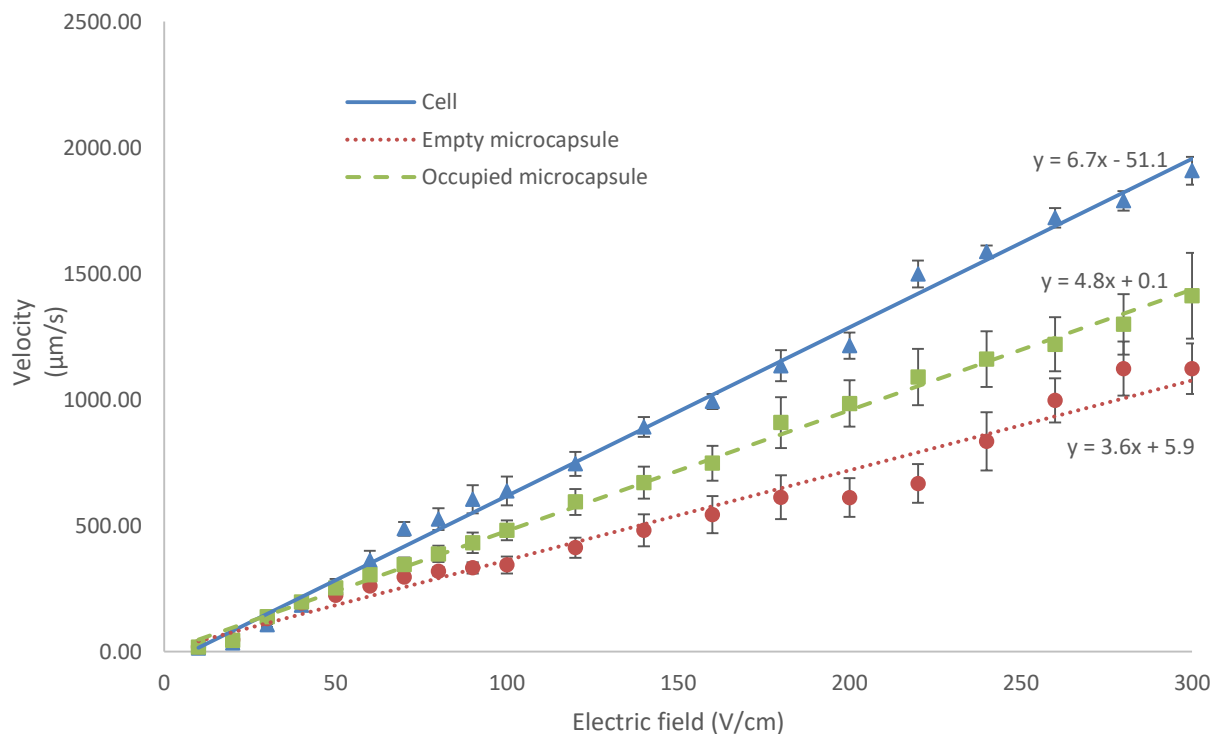
Figure 28: Electrophoretic velocities of cells, empty microcapsules, and occupied microcapsules at varying electric fields

During the characterization of occupied microcapsules, an interesting phenomenon was observed where microcapsules with an embedded cell extremely close to the edge reorient themselves while in motion, aligning the edge with cell to face the direction of the anode. In very limited cases, these cells break loose from their mother capsule and dash toward the anode leaving behind the slower-moving mother

45

capsule. Figure 29 shows a screenshot montage capturing a cell breaking out of a microcapsule as the microcapsule tries to orient itself.
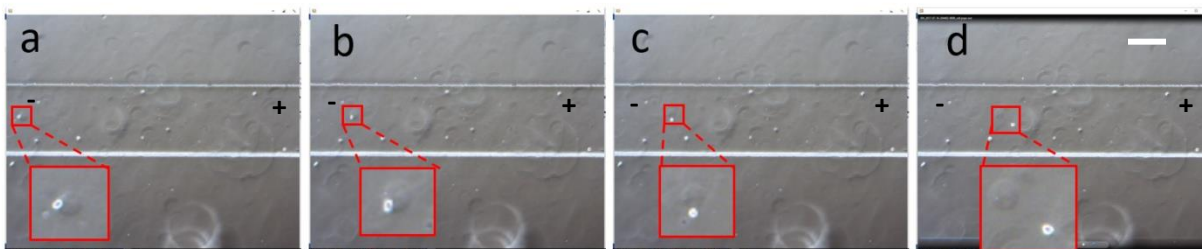
Figure 29: Screenshot sequence of a cell breaking out of a microcapsule under electric field of 50V/cm (scale bar = 250μm)

Even though cells, empty microcapsules, and occupied microcapsules all carry net negative charge, the graphs suggest notable differences in the magnitude of their mobilities. As implied by equations 16 and 16, electrophoretic mobility is directly proportional to particle charge, and the higher the electrophoretic mobility of a particle, the higher the velocity of electrophoretic motion. In other words, a particle carrying a larger charge will travel faster at a given electric field strength, provided that all other factors remain constant. By this logic, cell-laden microcapsules should have a higher net charge than empty microcapsules given that they travel faster at a set electric field. To confirm this, we have extracted relevant information pertaining to charge and electrophoretic mobilities from the graph. Table 1 summarises the net charges and electrophoretic mobilities of 3T3 cells, empty microcapsules, and occupied microcapsules as determined from the linear fit of velocity vs electric field plots in Figure 28, and also using equations 16 and 17.

By comparing the equation of the linear fit of the graphs to equation 18, the slope of the graphs represents electrophoretic mobility and knowing the electrophoretic mobility, we can calculate the net charge using equation 17. For the calculation of net charge, radius of microcapsules was set to the value of 25μm, while radius of 3T3 cells was set to the value of 9μm [62].

Table 1: Summary of average charge and electrophoretic mobility of 3T3 cells, empty microcapsules, and cell-laden microcapsules

Particle	Radius (µm)	Net Charge x10⁻¹¹ (Coulombs)	Electrophoretic Mobility x10⁻⁴ (cm²/V-s)
3T3 mouse fibroblast cells	9	1.14±0.02	6.7±0.1
Empty agarose microcapsules	25	1.68±0.07	3.6±0.2
Cell-laden agarose microcapsules	25	2.26±0.03	4.8±0.1

It is quite clear from the results shown in Table 1 that cell-laden microcapsules exhibit a higher mobility than empty microcapsules. We hypothesise that the presence of a cell in a microcapsule increases the microcapsule's net charge and consequently its electrophoretic mobility. This is a reasonable hypothesis given that cells have a higher charge concentration compared to agarose microcapsules, and it is only logical that embedding a cell in a microcapsule increases the net charge of the microcapsule.

The percentage volume of microcapsule occupied by cells also has a bearing on the net charge of a microcapsule. Figure 30 shows a plot of how the percentage volume of microcapsule occupied by a single 3T3 cell (18µm diameter) varies with different sizes of microcapsules.
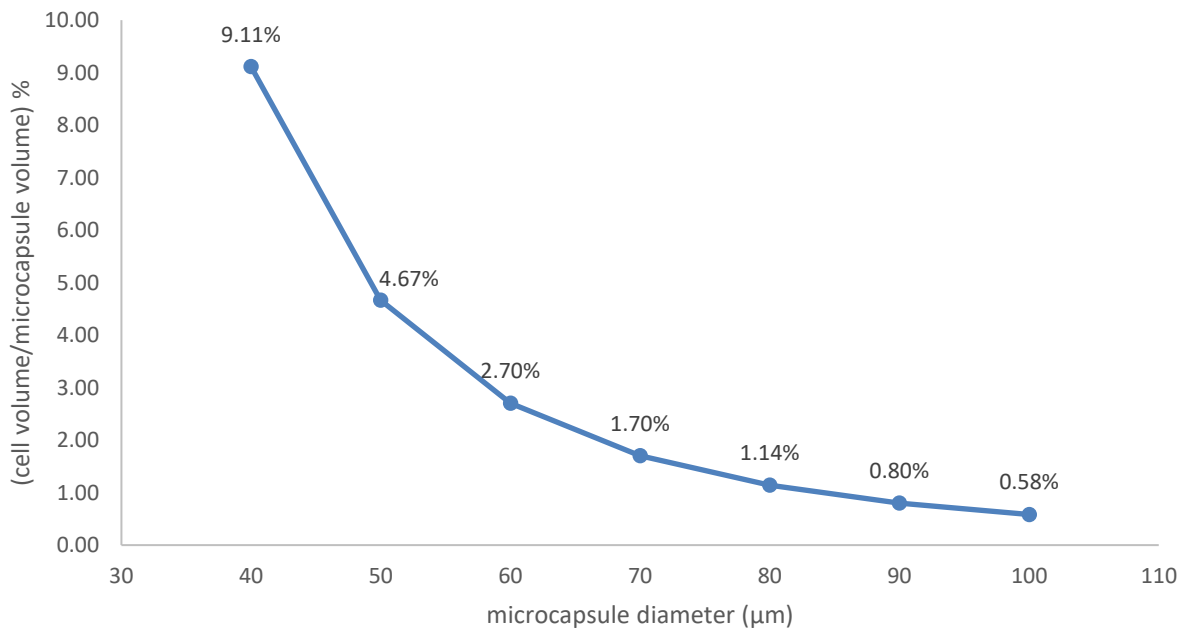
Figure 30: Cell-to-microcapsule volume ratio for different diameters of microcapsules

As the diameter of microcapsule increases, the percentage of microcapsule volume occupied by cells drops exponentially. For instance, by embedding a 3T3 cell within a microcapsule of 50µm diameter, approximately 4.67% of the microcapsule volume is being occupied, and if the diameter of the microcapsules is increased to 70µm, the percentage drops sharply to only 1.7%. This has an implication on electrophoretic sorting applications where a high cell to microcapsule volume ratio is highly desirable. A small microcapsule diameter, and consequently a low cell-to-microcapsule volume ratio, will enhance the contrast between cell-laden microcapsules and empty microcapsules, making the differential EP forces acting on the two groups of microcapsules larger.

Chapter 5

DIELECTROPHORETIC AND ELECTROPHORETIC SORTING OF MICROCAPSULES

5.1 DEP Sorting Principle

As explained in chapter 3, the DEP force experienced by a particle when subjected to a non-uniform electric field is dependent on factors such as the dielectric properties of the particle, the size of the particle, the electric field gradient, and dielectric properties of the surrounding media. If two particles of different dielectric properties, or of different sizes, are placed in a region of non-uniform electric field, both particle will experience a DEP force and if the DEP force is large enough, the particles will deviate from their original trajectories. However, the fact that they have different sizes or different dielectric properties will affect how much DEP force each particle experiences or which type of DEP force each particle experiences, whether it's negative or positive. Thus, the key to sorting particles based on DEP is to identify the right electric field gradient and frequency that will trigger different deflection patterns of the two particles. That is to find the right AC voltage and the right frequency where one particle experiences a greater deflection than the other particle.

5.2 Proposed DEP Sorting Technique Encapsulated Cells

Sorting of encapsulated cells can be achieved by exploiting differences in the frequency-dependent responses of cell-laden microcapsules and empty microcapsules. In chapter 3, we carried out characterization experiments where the frequency dependent DEP profiles of empty microcapsules and occupied microcapsules were plotted, see Figure 24. The experiment was based on 3T3 mouse fibroblast cells encapsulated in 2% agarose microcapsules of 50µm in diameter and suspended in low conductivity media (8.5% sucrose + 0.3% dextrose). Results showed notable variations in DEP forces experienced by

empty and occupied microcapsules in the frequency range of 150 kHz to 4 MHz as empty microcapsules experienced higher DEP force than cell-laden ones. This difference thus presents an excellent opportunity for sorting in the afore-mentioned frequency range. A microfluidic device with embedded planar electrode inside the microchannel can be designed such that when the appropriate sorting frequency is applied, empty microcapsules which experience higher DEP force are pulled towards the electrode and channelled out through an outlet while leaving occupied microcapsules experiencing weaker DEP force to flow out freely through an adjoining outlet. A demonstration of this concept is shown in Figure 31.
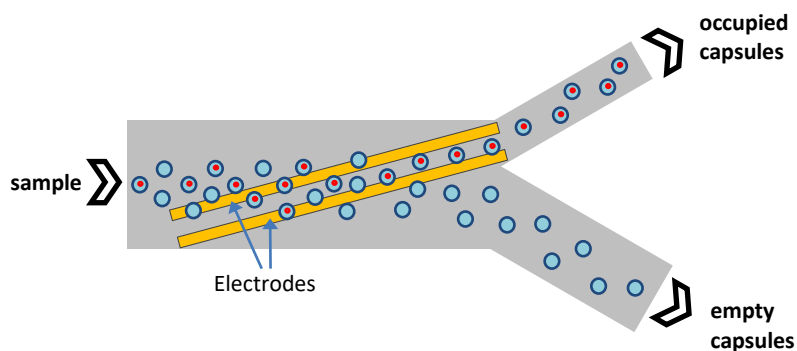
Figure 31: Illustration of DEP sorting principle of microcapsule

5.3   Proposed Device for DEP Sorting

In order to generate DEP forces inside microchannels in microfluidic devices, electrodes have to be integrated within the channels. One of the most practical way of doing this is to fabricate the electrode directly on the glass floor of the microchannels. Electrodes were made from patterning of glass slides that have been pre coated with 50nm thick gold on 5nm thick chromium adhesion layer. Details of fabrication steps in section 3.2. The shape and design of the electrode depends on its intended application.

The first generation DEP sorting device was designed by a former Post-Doctoral Fellow at the GodinLab, Dr. Benjamin Watts. The device (see Figure 32 a,b) combines DEP sorting downstream of microcapsule generation on the same microfluidic chip. The DEP module features two pairs of parallel electrodes cutting across a split microchannel and converging into an outlet at the tail end of the channel. Upon multiple testing of this device, we found that the two-electrode configuration is limited in handling a

high volume of microcapsules as microcapsules are crammed in the small gap between the two electrodes under the influence of DEP force.

To correct the limitation of narrow effective DEP surface area in the first generation design, a second generation design was proposed (Figure 32 c,d). The device incorporates an interdigitated electrode design. Interdigitated electrodes have the advantage of maximizing the effective DEP surface area within a fluidic channel. This design was inspired by a device proposed by Song et al [17] for the separation of human mesenchymal stem cells (hMSC) from their progenies; the major difference being that the width of the electrode fingers in our design was made larger and likewise the spacing between interdigitated fingers.
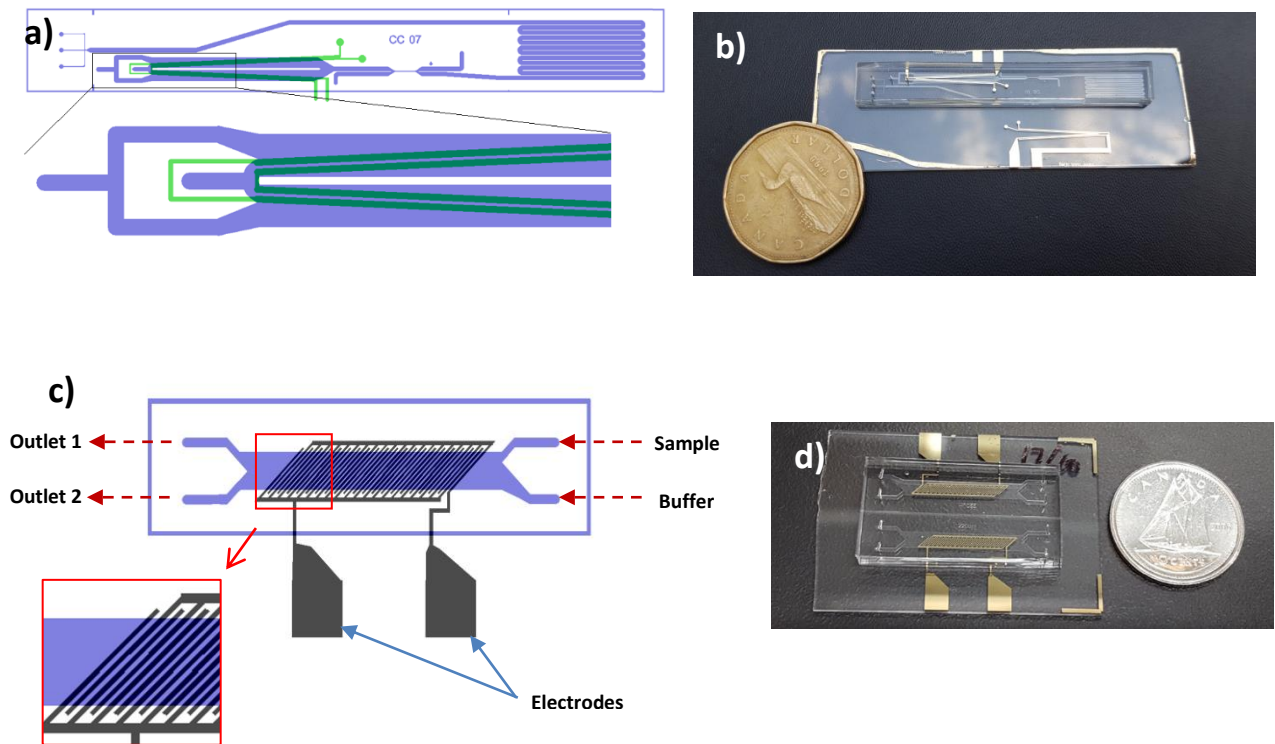
Figure 32 a) Schematic of first generation DEP microcapsule sorting device ©Benjamin Watts; b) Picture of first generation DEP microcapsule sorting device next to a 1 Canadian dollar coin; c) Schematic of proposed 2nd generation device for DEP microcapsule sorting. Device consists of interdigitated electrodes lining the floor of the flow channel aligned at 45 degrees to the direction of flow. Electrodes are 100µm wide and spaced apart by 200µm. Flow channel is 2mm wide and 15mm long; d) Picture of two adjoining sorting devices next to a 10 Canadian cent coin.

As shown in Figure 32c, a sample mixture of empty and occupied microcapsules in low conductivity media is introduced to the device through the top right inlet. A buffer solution of low conductivity is introduced through the bottom right channel. The purpose of the buffer solution is to help focus and streamline the flow of the sample mixture. The two liquids flow parallel to one another in a laminar

manner. AC electric fields are delivered to the channel through the two electrode pads. When the AC signal is turned off, the sample mixture of empty and occupied microcapsules are carried by hydrodynamic drag in a straight line trajectory (see Figure 33a) through the channel and exit through the top left outlet as shown in Figure 33a. However when AC signal is turned on and set to a predetermined sorting voltage and frequency, microcapsules experiencing greater DEP are gradually deflected across the channel as they travel and eventually exit through the bottom left channel (see Figure 33b). Microcapsules experiencing weak DEP force are overwhelmed by hydrodynamic drag and keep flowing in a straight line, exiting through the top left channel. Given that empty microcapsules experience greater DEP force at 150 kHz to 4MHz according to results presented in Chapter 3, we expect them to be deflected downwards while occupied microcapsules continue moving in a straight line as shown in Figure 33b.

a) DEP **off**   b) DEP **on**
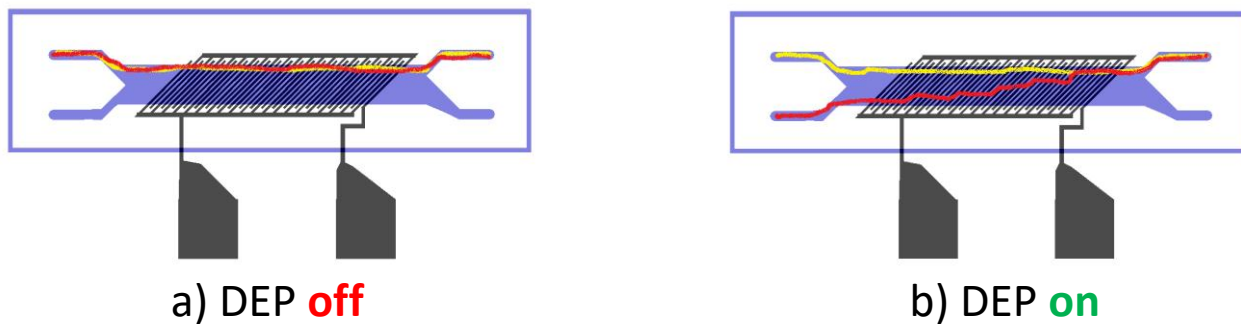
Figure 33: Pattern of flow of occupied microcapsules and empty microcapsules when DEP is turned off versus when turned on

5.4   Preliminary Testing of DEP Sorting Devices and Observations

The first set of experiments was aimed at deflecting empty microcapsules using the first generation device which combines droplet generation with DEP sorting in a continuous stream. Microcapsules were formed using 2% (m/V) agarose containing 20% (V/V) DPBS. While testing this device, some notable observations were made.

Problem 1: Clumping of Microcapsules

First, we observed that when AC signal is applied to the electrode, microcapsules that come in contact with the electrode clump together. A picture of this phenomenon was captured and shown in Figure 34. This effect was observed at voltages greater than 5V and across the frequency range of 150kHz up to

about 5MHz, however at higher voltages (above 40V), the microcapsule clumps turn into giant masses of melted agarose. We later found this effect to be due to the fact that the microcapsules were still submerged in oil from the encapsulation stage which continued downstream to the DEP stage. Once oil is removed before applying electric field, the clumping phenomenon disappears.
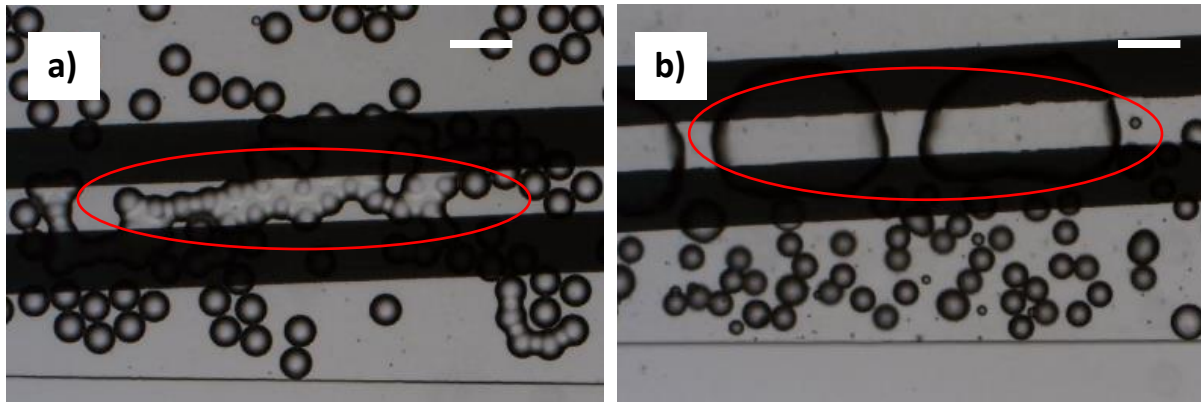
Figure 34: Microscope captures showing clumping of microcapsules when suspended in oil DEP force at (a) 8Vpp 1MHz; (b) 70Vpp 1MHz [scale bars = 100µm]

Problem 2: Electrode Degradation

We observed that at high voltages (above 70V), the melting of agarose microcapsules suspended in oil (Figure 34b) causes a vigorous reaction in the microchannel that causes degradation of the electrodes (Figure 35). A possible explanation for the electrode degradation is galvanic corrosion. Galvanic corrosion occurs when two electrode are shorted by an electrolyte under the application of electric field whereby the electrodes exchange ions with the electrolyte causing decay of the electrodes. In this case, the Ag/Cr electrodes are shorted by ion-rich DPBS released into the microchannel by the melted agarose microcapsules which acts as electrolyte. The electrolyte-electrode combination forms a galvanic couple.
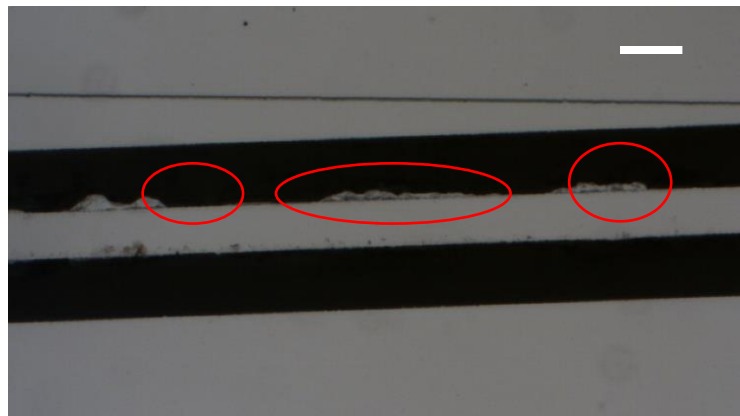
Figure 35: Electrode degradation due to galvanic coupling [scale bar = 100µm]

When low conductivity media was used in place of DPBS, the galvanic corrosion effect disappeared. Once the two problems were addressed, we were able to demonstrate DEP deflection and channeling of empty microcapsules to an outlet with an AC signal of 70V at 1MHz. This is shown in Figure 36.
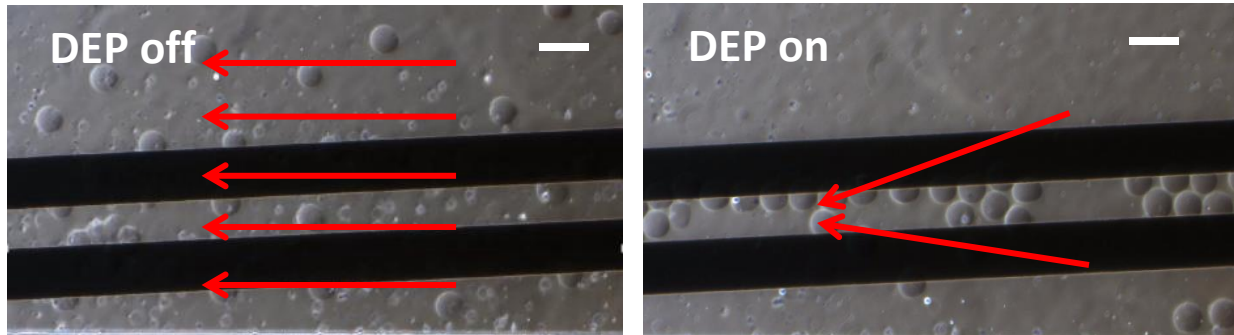
Figure 36: Microscope captures showing deflection of microcapsules into the space between electrodes when DEP is turned on and dispersion of microcapsules across the channel when DEP is turned off [scale bars = 100μm]

DEP Sorting of Microcapsules

After experimenting with empty microcapsules, the next step was to attempt sorting microcapsules containing cells from ones that are empty in the sorting frequencies identified in Chapter 3. Much of the experiments in this regard were performed using the second generation device shown in Figure 32c. These experiments did not quite yield a visible separation of the microcapsules. A possible explanation for this is that the interdigitated electrode design is not capable of sorting at a frequency where both empty microcapsules and occupied microcapsules are experiencing DEP forces in the same direction (i.e. positive DEP force) even though the magnitude of those forces are different. A potential solution might be to run more characterization experiments for frequencies outside the already tested range of 150kHz to 7MHz to find a frequency where one group of microcapsules experiences positive DEP force and the other group experiences negative DEP force, and sort at that frequency. Another potential solution is to completely redesign the electrodes such that they can discriminate between empty and occupied microcapsules that are experiencing DEP forces in the same direction but of different magnitudes.

5.5   EP Sorting Principle

In chapter 4, it was shown that the electrophoretic force experienced by a particle when subjected to a DC electric field is proportional to the charge of the particle. It was also shown that the higher the

particle charge, all other factors being the same, the higher the velocity of the induced electrophoretic motion of the particle. The velocity of motion relative to electric field is denoted by a factor known as electrophoretic mobility. By taking advantage of differences in electrophoretic mobilities of two particles, the faster deflected particle can be channeled into an outlet while the slower deflected particle can be channeled into another outlet.

5.6   EP Sorting of Encapsulated Cells Principle

With sorting in mind, the electrophoretic responses of empty microcapsules as well as occupied microcapsules containing cells were determined where the velocity of motion of microcapsules were plotted against varying electric field strengths. Results (Figure 28) showed notable differences in the response of empty microcapsules and occupied microcapsules as occupied microcapsules experienced stronger EP force for a given electric field strength and travelled faster as a result. This difference is reflected in their respective electrophoretic mobilities as deduced from the graph as occupied microcapsules had higher electrophoretic mobilities than occupied microcapsules.

The difference in electrophoretic mobilities presents an excellent advantage for the separation of empty microcapsules from occupied ones. Given that occupied microcapsules travel faster than empty microcapsules at a set electric field, they will exhibit a steeper lateral deflection (Δy_o) than empty microcapsules (Δy_e) as they flow through a microchannel if electric field is applied across the channel width (see Figure 37). Occupied microcapsules with larger deflection exit through the bottom outlet while occupied microcapsules with smaller deflection exit through the top outlet.
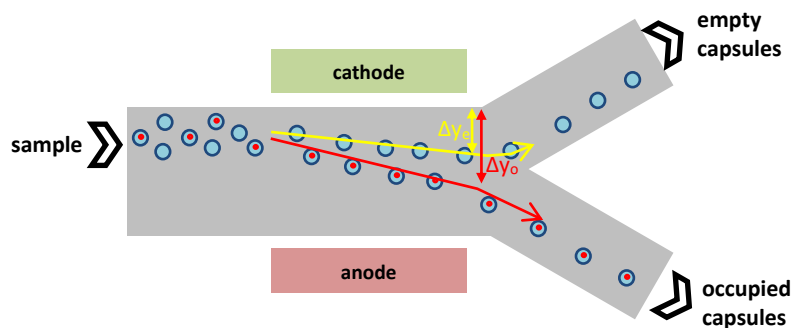
Figure 37: Illustration of EP sorting principle of microcapsule

5.7   Proposed EP Sorting Devices

The proposed first generation sorting device is shown in Figure 38. The device features a fluidic channel 300µm wide and 6000µm long. The fluidic channel is flanked by 500µm wide electrode channels separated by PDMS spacing of 100µm in which multiple 20µm wide tunnels were created to link the electrode to the fluidic channel. Pre-sorted microcapsule samples suspended in LCM are introduced into the device through the top left channel while a buffer solution of LCM is introduced through the bottom left channel. Sorted microcapsules are collected in via the two outlets at the end of the fluidic channel. Electrodes were fabricated using Cerrolow 117 low melt alloy. The protocol for electrode fabrication is provided in the appendix.
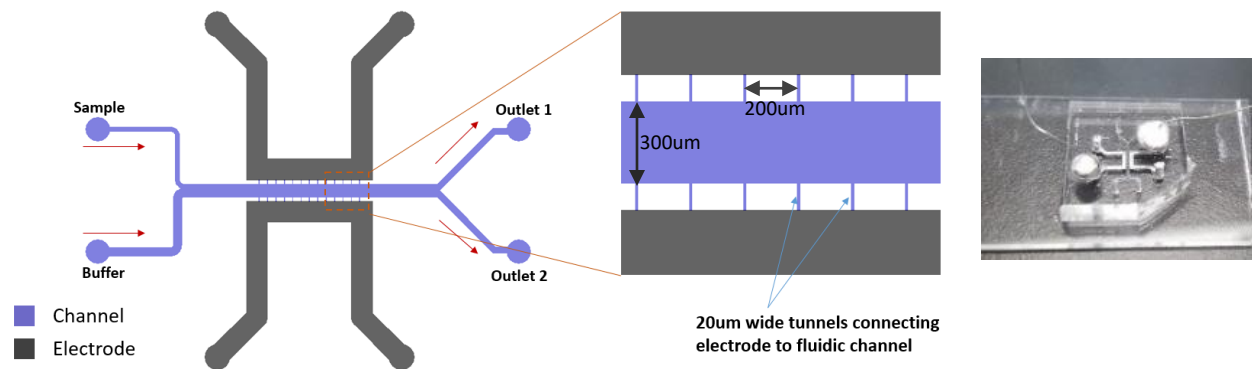
Figure 38: Schematic and photograph of proposed EP sorting device.

5.8   Preliminary Testing of EP Sorting Devices and Observations

The first experiment performed was to validate the proposed ED sorting device. Polystyrene microbeads of 5um diameter (Model: Bangs Laboratories) were passed through the device and subjected to a DC electric field of 20V/cm. These microbeads carry a net negative charge as a result of the adsorption of negatively charged alkyl sulfonates and sulfates during emulsion polymerization at manufacturing [63]. Upon the application of electric field, the microbeads were deflected diagonally across the channel as shown in Figure 39 ad exit out through the bottom right outlet. When electric field is off, microbeads move in a straight line along the top edge of the channel and exit through the top right outlet.
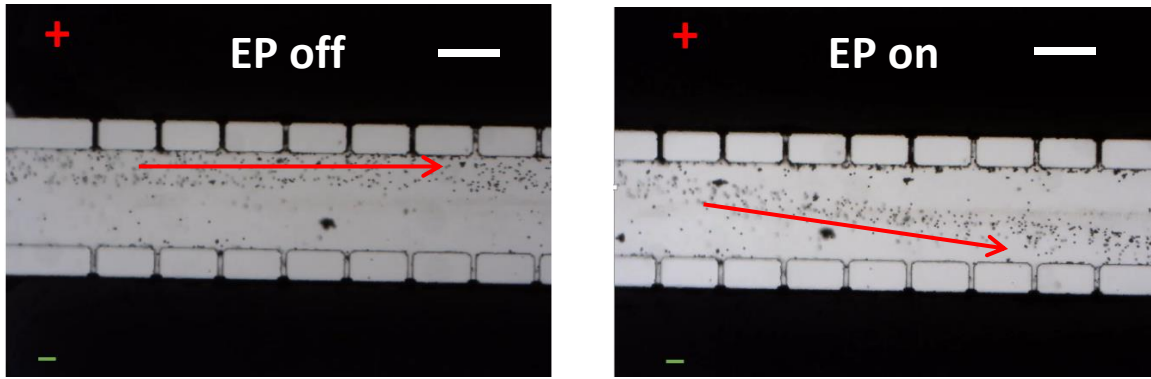
Figure 39: Deflection of polystyrene microbeads when subjected to electrophoretic force due to a DC field of 20V/cm [scale bar = 200μm]

After testing with polystyrene beads, EP deflection and separation of empty microcapsules from microcapsules containing 3T3 mouse fibroblast cells was then attempted using the proposed device. Microcapsules were formed using 2% (m/V) agarose containing 20% (V/V) DPBS. Results showed successful deflection of microcapsules at a very low flow velocity of approximately 500μm/s and an applied voltage of 5V. As shown in Figure 40, when EP force is applied, microcapsules entering the channel through the top left inlet are deflected laterally to the opposite side of the channel and eventually exit through the bottom right outlet. However at very high flow rates, greater than 5000μm/s, hydrodynamic force seems to overcome EP force and the microcapsules all move in a straight line and exit through the top right outlet. Conversely when EP force is significantly stronger than hydrodynamic force, the microcapsules stick to the open grooves in the channel that links it to the electrode (see Figure 41).
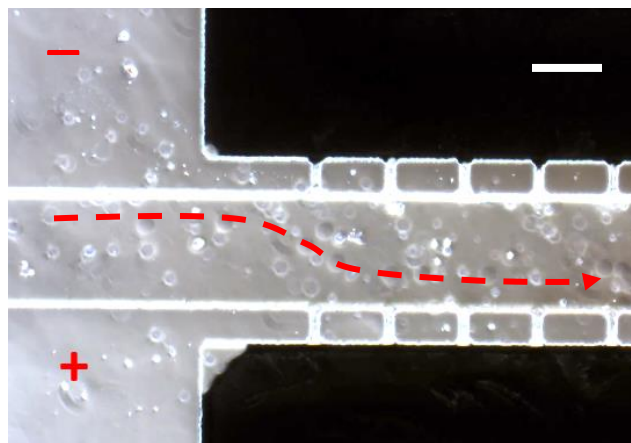
Figure 40: Deflection of empty and occupied microcapsules to opposite side of microchannel due to EP force [scale bar = 200μm]

Even though microcapsules were successfully deflected, there did not seem to be a significant difference in the deflection patterns between empty microcapsules and occupied microcapsules making it impossible to sort with this current device. As can be seen in Figure 40, both sets of microcapsules appear to be deflected in a similar trajectory, as wells as migrate out through the same outlet. In retrospect, the fluidic channel could have been designed much wider. A wider channel would allow for a better defined set of trajectories for the movement of the two sets of microcapsules, having shown that they possess different electrophoretic mobilities. Futhermore, a wider would reduce the chances of both trajectories recombining on the opposite side of the channel before reaching the outlets.
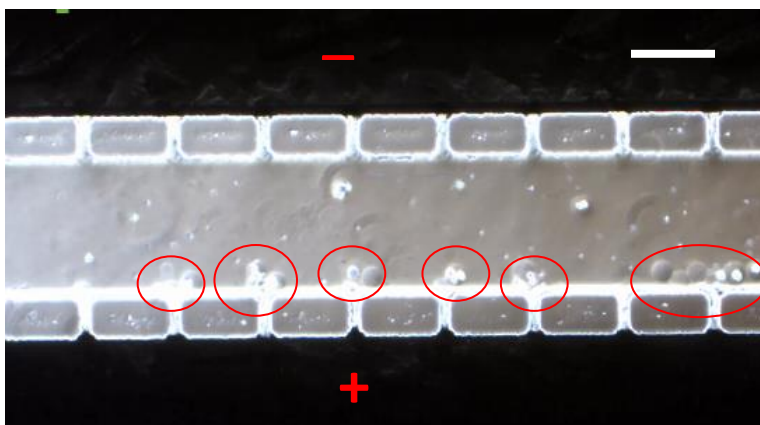
Figure 41: Microcapsules sticking to openings of the tiny channels linking the main fluid channel to electrode [scale bar = 200μm]

5.9   Proposed re-designed EP sorting device

The first generation EP sorting device shown in Figure 38 was designed with a 6000μm long and 300μm wide fluidic channel. These dimensions were chosen based on empirical estimations. However upon testing, we found that that the 300μm channel width is too narrow relative to the 50μm diameter of the microcapsules. As a result, both groups of microcapsules (empty and occupied) when subjected to electric field, deflect laterally and end up converging at the opposite side of the channel before reaching the outlet. In order to address this issue, a new design for a future second generation EP sorting device is proposed (see Figure 42).

The second generation sorting device takes into account four interdependent parameters:

1. flow velocity
2. electric field
3. channel length
4. channel width

In designing the fluidic channel, we started by selecting a reasonable arbitrary value for channel length, followed by a desirable flow velocity, and an electric field strength to be used for sorting. Using these pre-selected parameters in combination with the electrophoretic mobility graph in Figure 28, we found the respective y-axis displacement of occupied microcapsules and that of empty microcapsules after travelling the entire length of the channel. The channel width and the location of the outlet divider were then specified based on the expected displacements of sorted microcapsules.

For the proposed second generation device shown in Figure 42, the following parameters were used to determine the ideal width of the channel and the location of the outlet divider as shown in Figure 43.

- *Channel length (l)* = 10,000µm

- *Flow velocity (v_{flow}) = 5,000μm/s*
- *Electric field (E) = 200V/cm; [at 200V/cm, respective EP velocities of empty capsules and occupied capsules are: v_e = 720μm/s; v_o = 960μm/s (from the graph in Figure 28)]*
- *Empty capsule displacement (Δy_e) = ?*
- *Occupied capsule displacement (Δy_o) = ?*
- *Channel width (w) = ?*
- *Outlet divider location (y_D) = ?*
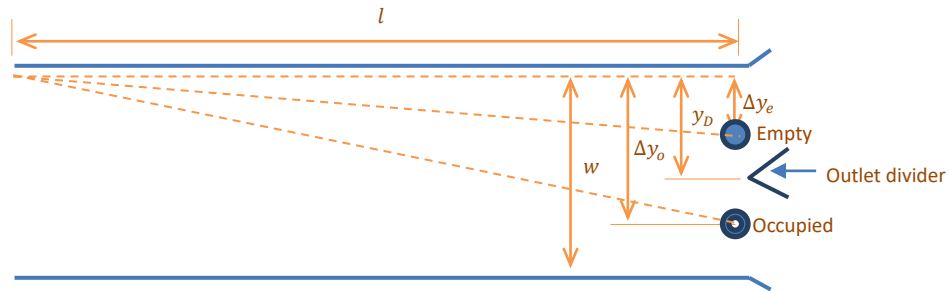
Figure 43: Schematic showing expected displacement patterns of empty and occupied microcapsules as well as the placement of outlet divider relative to the width of the channel

To find the displacement of microcapsules at the end of the channel under a transverse electric field across channel width, we first find the time, t, it takes capsules to travel along channel length from one end to the other given the flow velocity, $v_{flow.}$

$$t = \frac{l}{v_{flow}} = \frac{10000\mu m}{5000\mu m/s} = 2s$$

Knowing the time it takes capsules to reach the end of channel as calculated above, and the EP velocities of empty and occupied microcapsules at an applied electric field of 200V/cm from Figure 28, we can find their respective lateral displacements as follow:

$$\Delta y_e = v_e t = 720\mu m/s \times 2s = 1440\mu m$$

$$\Delta y_o = v_o t = 960\mu m/s \times 2s = 1920\mu m$$

Given the calculated displacements, we can specify the location of the outlet divider, y_D, as well as the width of the channel, w (see Figure 43). Ideally we want to place a divider halfway between Δy_e and Δy_o, at $y_D = (\Delta y_e + \Delta y_o)/2$. The channel width, w, is then specified at $2y_D$.

$$y_D = \frac{\Delta y_e + \Delta y_o}{2} = \frac{1440\mu m + 1920\mu m}{2} = 1680\mu m$$

$$w = 2y_D = 3360um$$

5.10 Cell Viability

The viability of cells after exposure to DEP and EP forces was not studied in this thesis. However, several studies have shown that exposure of cells to DEP electric fields for a very few seconds as is the case with our DEP experiments, has an insignificant impact on cell viability [17] [64], and that DEP only becomes hazardous when cells are continuously exposed to AC fields for a prolonged period of time in the order of hours [65]. Yang et al [65] demonstrated that there is almost a non-change in viable cell numbers when Lysteria monocytogene cells were exposed to a DEP field of 20Vpp at 5MHz for 60 minutes, whereas viability plunged anywhere from 56.8% to 75.8% after cells have been exposed to DEP field continuously for 4 hours. Similarly for EP, studies have shown that a good cell viability can be maintained even at a relatively high DC electric field of 100V/cm for a relatively prolonged cell exposure duration of 5 minutes [66]. Nordling et al [66] performed viability studies on T and B lymphocytes after sorting them electrophoretically with the cells exposed to 100V/cm DC fields for 300 seconds, and was able to demonstrate that more than 90% of cells remained viable after exposure and that these cells went on to carry out regular biological functions which indicated that they were alive and healthy. In contrast to Nordling et al's parameters, our future proposed EP sorting experiment in section 5.9 uses a DC electric field of 200V/cm at very short exposure duration of 2 seconds determined by the flow velocity.

Chapter 6

CONCLUSION AND OUTLOOK

6.1   Conclusion

Cell encapsulation is a rapidly developing concept in stem cell therapies and regenerative medicine. It has shown the potential to boost the therapeutic effects of such treatments, owing to several advantages such as improved viability and survival rates of stem cells in capsules after transplant. Microfluidic-based technique is emerging as one of the most preferred methods of encapsulation given that it is able to produce uniformly sized microcapsules, allows for control over the size of microcapsules, and can yield a high throughput. However, despite these advantages, the random nature of encapsulation in the microfluidic method means that yielded samples contain a mixture of cell-laden microcapsules and an undesired amount of empty microcapsules. In order to purify samples, there is a need to separate empty microcapsules from cell-laden ones. Dielectrophoresis (DEP) and electrophoresis (EP) are two of the commonly used methods for particle sorting on microfluidic platforms because they allow for label-free sorting and yield a high throughput. Table 2 summarizes the differences between these two phenomena with respect to the sorting of microcapsules or any other micro-particle.

Table 2: Summary of the distinguishing factors between DEP and EP

	DEP	EP
Particle charge	Microcapsules/particles can be neutrally, positively, or negatively charged	Microcapsules/particles must carry a net positive or net negative charge
Electric field	Requires a non-uniform AC electric field	Requires a uniform DC electric field
Variables	Magnitude of DEP force depends on microcapsule size, dielectric	Magnitude of EP force depends on net charge of microcapsules as well

	properties of microcapsules and medium, magnitude and frequency of applied AC field	as the magnitude of the applied DC field
Ideal sorting scenario	Can be used to sort microcapsules ideally by applying the frequency where one group of capsules to be sorted experiences negative DEP while the other group experiences positive DEP	Can be used for sorting microcapsules ideally if the mixture to be sorted consists of one group of capsules that is positively changed and another group that is negatively charged
Characterization objective	To identify the frequency where the two groups of microcapsules to be sorted experience widely different DEP forces, ideally of opposite polarities	To identify the net charges and the electrophoretic mobilities of the two groups of microcapsules

In this thesis, a technique for characterizing DEP effects on microcapsules using hydrodynamic flow was proposed. The DEP characterization experiments aimed to find the DEP forces experienced by empty microcapsules and cell-laden microcapsules over a frequency bandwidth in low conductivity medium. Frequency ranges between 150 kHz and 7 MHz were successfully characterized with an applied peak-to-peak voltage of 40V. Result showed that empty microcapsule experience higher DEP forces than occupied ones between 150 kHz and 2 MHz. However, from 2 MHz to 7 MHz, they both experience similar DEP forces. This leads us to conclude that there is a potential for the successful sorting of microcapsules using DEP in the frequency range of 150 kHz to 2 MHz. Nonetheless, an ideal sorting frequency is where one group of microcapsules experience positive DEP and the other group experience negative DEP. This frequency was not identified in this experiment between the tested range of 150 kHz to 7 MHz.

Furthermore, a method for characterizing the EP response of microcapsules was proposed. The EP characterization experiments aimed to find the electrophoretic mobilities of both empty and cell-laden microcapsules. Velocities of EP motion of microcapsules were measured over a range of electric field strengths. Electrophoretic mobility data were extracted from the graph of EP velocity against electric field. Results showed that agarose microcapsules are negatively charged, with cell-laden microcapsules being more negatively charged and thus possess a higher electrophoretic mobility at a neutral pH than empty microcapsules. The electrophoretic mobility of cell-laden microcapsules in a low conductivity media was found to be $4.8(\pm0.1)\times10^{-4}$ cm^2/V-s, meaning that a microcapsule containing a single cell will

travel at a velocity of 4.8(±0.1) μm/s in an electric field of 1V/cm. In contrast, the electrophoretic mobility of empty microcapsules was found to be 3.6(±0.2)x10^{-4} cm^2/V-s meaning that an empty microcapsule will travel at a velocity of 3.6(±0.2) μm/s in an electric field of 1V/cm.

In addition to the work described on the characterization of DEP and EP forces on microcapsules, some potential sorting devices that take advantage of these electrokinetic phenomena were likewise proposed. The ultimate goal of performing electrokinetic characterization on microcapsules is to capture useful data that can be leveraged for sorting empty microcapsules from ones containing cells, and this work sets a useful foundation for that.

6.2   Outlook

Further work needs to be carried out in certain areas in order to improve on current results presented in this thesis. In this final section of the report, we have highlighted areas for possible future improvements.

6.2.1   Outlook on DEP Characterization and Sorting of Microcapsules

The experiments described herein for the DEP characterization of microcapsules revealed how microcapsules respond to DEP forces over a range of frequencies. However, these experiments provided a limited insight given that negative DEP could not be characterized with the current device, and that certain frequency ranges below 150 kHz could not be characterized due to equipment limitation. A future direction would be to design new sets of devices with the capability to measure negative DEP. By being able to measure negative DEP and positive DEP on a single device, it will be easy to identify the cross-over frequencies of empty microcapsules and cell-laden microcapsules. A cross-over frequency is the frequency at which the DEP force experienced by a particle transitions from positive to negative or vice versa. Essentially at the cross over frequency, the DEP force experienced by a particle is equal to zero. Identifying the cross-over frequency presents a significant advantage for sorting cell-laden DEP microcapsules from empty ones. If the cross-over frequencies are found to be significantly different, occupied microcapsules and empty microcapsules can be sorted by selecting the frequencies that generate a positive DEP force for one group and a negative DEP force for the other group, thus creating

a divergent force for separation. Positive DEP implies that microcapsules will be attracted to the electrode while negative DEP means that microcapsules will be repelled away from the electrodes.

6.2.2 Outlook on EP Characterization and Sorting of Microcapsules

The EP characterization experiments showed that occupied microcapsules exhibit a close electrophoretic mobility to empty microcapsules at a neutral pH. A worthwhile future investigation would be to modify the net charge of agarose and/or cells, and observe how electrophoretic mobility values change. One way to accomplish this is through isoelectric focusing. Isoelectric focusing is a popular concept in gel electrophoresis which is used in the separation of DNA strands. The concept involves tuning the charge of molecule by adjusting the pH of the medium in which the particle is suspended. By making the medium more acidic, the molecule is made more positive, and by making the medium more alkaline, the charge of the molecule is made more negative. This same concept can be borrowed over for microcapsule sorting. By performing isoelectric focusing on cells, or on agarose capsules, we can enhance the differences in net charge of agarose relative to cells, making it easier to sort. As of present, there are studies that have performed isoelectric focusing on cells and have demonstrated that cells exhibit an increase in net negative charge when suspended in an alkaline medium and therefore possess a higher electrophoretic mobility as a result [31]. Electrophoretic sorting of cell-laden microcapsules can be made more efficient if the net charge of cells can be adjusted through isoelectric focusing to make them more negative relative to agarose, or vice versa.

REFERENCES

[1] J. F. Edd, D. Di Carlo, K. J. Humphry, S. Koster, D. Irimia, D. A. Weitz and M. Toner, "Controlled Encapsulation of Single-cells into Monodisperse Picoliter Drops," *Lab on a Chip,* vol. 8, pp. 1262-1264, 2008.

[2] A. E. Mayfield, E. L. Tilokee, N. Latham, B. McNeill, B.-K. Lam, M. Ruel, E. J. Suuronen, D. W. Courtman, D. J. Stewart and D. R. Davis, "The effect of encapsulation of cardiac stem cells within matrix enriched hydrogel capsules on cell survival, post-ischemic cell retention and cardiac function," *Biomaterials,* vol. 35, no. 2014, pp. 133-142, 2013.

[3] R. M. Olabisi, "Cell microencapsulation with synthetic polymers," *Journal of Biomedical Materials Research,* vol. 2015, no. 103A, pp. 846-859, 2015.

[4] G. Orive, R. M. Hernandez, A. R. Gascon, R. Calafiore, T. M. S. Chang, P. de Vos, G. Hortelano, D. Hunkeler, I. Lacik and J. L. Pedraz, "History, Challenges and Perspectives of Cell Microencapsulation," *Trends in Biotechnology,* vol. 22, no. 2, pp. 87-92, 2004.

[5] J.-M. Zhang and J. An, "Cytokines, Inflammation and Pain," *International Anesthesiology Clinics,* vol. 45, no. 2, pp. 27-37, 2007.

[6] H. Uludag, P. De Vos and P. A. Tresco, "Technology of Mammalian Cell Encapsulation," *Advanced Drug Delivery Reviews,* vol. 42, pp. 29-64, 2000.

[7] J. Koo and T. M. Chang, "Secretion of Erythropoietin from Microencapsulated Rat Kidney Cells: Preliminary Results," *International Journal of Artificial Organs,* vol. 16, no. 7, pp. 557-560, 1993.

[8] S. Prakash and T. M. Chang, "Microencapsulated Genetically Engineered Live E.Coli DH5 Cells Administered Orally to Maintain Normal Plasma Urea Level in Uremic Rats," *Nature Medicine,* vol. 2, no. 8, pp. 883-887, 1996.

[9] Y. Sun, X. Ma, D. Zhou, I. Vacek and A. M. Sun, "Normalization of diabetes in spontaneously diabetic cynomologus monkeys by xenografts of microencapsulated porcine islets without immunosuppression," *Journal of Clinical Investigations,* vol. 98, no. 6, pp. 1417-1422, 1996.

[10] G. Hortelano, A. Al-Hendy and P. L. Chang, "Delivery of Human Factor IX in Mice by Encapsulated Recombinant Myoblasts: A Novel Approach Towards Allogeneic Gene Therapy of Hemophilia B.," *Blood,* vol. 87, no. 12, pp. 5905-5103, 1996.

[11] J.-M. Rabanel, X. Banquy, H. Zouaoui, M. Mokhtar and P. Hildgen, "Progress technology in microencapsulation methods for cell therapy," *Biotechnology Progress,* vol. 25, no. 4, pp. 946-963, 2009.

[12] H. Shintaku, T. Kuwabara, S. Kawano, T. Suzuki, I. Kanno and H. Kotera, "Micro cell encapsulation and its hydrogel-beads production using microfluidic device," *Microsystem Technology,* vol. 13, pp. 951-958, 2007.

[13] J. Clausell-Tormos, D. Lieber, J.-C. Baret, A. El-Harrak, O. Miller, L. Frenz, J. Blouwolff, K. J. Humphry, S. Koster, H. Duan, C. Holtze, D. Weitz, A. Griffiths and C. Merten, "Droplet-based Microfluidic Platforms for the Encapsulaion and Screening of Mammalian Cells and Multicellular Organism," *Chemistry and Biology,* vol. 15, pp. 427-437, 2008.

[14] D. J. Collins, A. Neild, A. deMello, A.-Q. Liu and Y. Ai, "The Poisson distribution and beyond: methods for microfluidic droplet production and single cell encapsulation," *Lab on a Chip,* vol. 2015, no. 15, pp. 3439-3459, 2015.

[15] L. Mazutis, J. Gilbert, W. L. Ung, D. A. Weitz, A. D. Griffiths and J. A. Heyman, "Single-cell analysis and sorting using droplet-based microfluidics," *Nature Protocols,* vol. 8, no. 5, pp. 870-891, 2013.

[16] C. Wyatt Shields IV, C. D. Reyes and G. P. Lopez, "Microfluidic cell sorting: a review of the advances in the separation of cells from debulking to rare cell isolation," *Lab on a Chip,* vol. 2015, no. 15, pp. 1230-1249, 2015.

[17] H. Song, J. M. Rosano, Y. Wang, C. J. Garson, B. Prabhakarpandian, K. Pant, G. J. Klarmann and A. Perantoni, "Continuous-flow sorting of stem cells and differentiation products based on dielectrophoresis," *Lab on a Chip,* vol. 2015, no. 15, pp. 1320-1328, 2015.

[18] M. D. Pysher and M. A. Hayes, "Dielectrophoretic Sorting of Particles and Cells in a Microsystem," *Analytical Chemistry,* vol. 79, no. 12, pp. 4552-4557, 2007.

[19] T. Franke, A. Abate, D. Weitz and A. Wixforth, "Surface acoustic wave (SAW) directed droplet flow in microfluidics for PDMS devices," *Lab on a Chip,* vol. 9, no. 18, pp. 2625-2627, 2009.

[20] L. Schmie, D. A. Weitz and T. Franke, "Sorting drops and cells with acoustics: acoustic microfluidic fluorescence-activated cell sorter," *Lab on a Chip,* vol. 2014, no. 14, pp. 3710-3718, 2014.

[21] B. Landenberger, H. Höfemann, S. Wadled and A. Rohrbacha, "Microfluidic sorting of arbitrary cells with dynamic optical tweezers," *Lab on a Chip,* vol. 2012, no. 12, pp. 3177-3183, 2012.

[22] O. Brzobohatý, V. Karásek, M. Šiler, L. Chvátal, T. Cizmar and P. Zemánek, "Experimental demonstration of optical transport, sorting and self-arrangement using a 'tractor beam'," *Nature Photonics,* vol. 7, no. 2, pp. 123-127, 2013.

[23] E. Brouzes, T. Kruse, R. Kimmerlin and H. H. Strey, "Rapid and continuous magnetic separation in droplet microfluidic devices," *Lab on a Chip,* vol. 2015, no. 15, pp. 908-919, 2015.

[24] J. McGrath, M. Jimenez and H. Bridle, "Deterministic lateral displacement for particle separation: a review," *Lab on a Chip,* vol. 2014, no. 14, pp. 4139-4158, 2014.

[25] M. D. Vahey and J. Voldman, "An Equilibrium Method for Continuous-Flow Cell Sortiong Using Dielectrophoresis," *Analytical Chemistry,* vol. 80, pp. 3135-3143, 2008.

[26] H.-D. Xi, H. Zheng, W. Guo, A. M, Gañán-Calvo and Y. A, "Active droplet sorting in microfluidics: a review," *Lab on a Chip,* vol. 2017, no. 17, pp. 751-771, 2017.

[27] H. A. Pohl and J. S. Crane, "Dielectrophoresis of cells," *Biophysical Journal,* vol. 11, pp. 711-727, 1971.

[28] B. J. Kirby, Micro- and Nanoscale Fluid Mechanics - Transport in Microfluidic Devices, Cambridge: Cambridge University Press, 2010.

[29] L. M. Broche, K. F. Hoettges, S. L. Ogin, G. E. N. Kass and M. P. Hughes, "Rapid, automated measurement of dielectrophoretic forces using DEP-activated microwells," *Electrophoresis,* vol. 32, pp. 2393-2399, 2011.

[30] K. V. 1. S. Kaler and T. B. Jones, "Dielectrophoretic spectra of single cells determined by feedback-controlled levitation," *Biophysics,* vol. 57, pp. 173-182, 1990.

[31] M. A. Witek, S. Wei, B. Vaidya, A. A. Adams, L. Zhu, W. Stryjewski, R. L. McCarley and S. A. Soper, "Cell transport via electromigration in polymer-based microfluidic devices," *Lab on a Chip,* vol. 4, no. 5, pp. 464-472, 2004.

[32] D. DiCarlo, "Inertial Microfluidics," *Lab on a Chip,* vol. 9, pp. 3038-3046, 2009.

[33] E. Lauga, M. Brenner and H. Stone, "Microfluidics: The No-Slip Boundary Condition," in *Springer Handbook of Experimental Fluid Mechanics*, Berlin, Springer, 2007, pp. 1219-1240.

[34] C. F. Gonzalez and V. T. Remcho, "Harnessing dielectric forces for separations of cells, fine particles and macromolecules," *Journal of Chromatography,* vol. 1079, no. 2005, pp. 59-68, 2005.

[35] S. Fiedler, S. G. Shirley, T. Schnelle and G. Fuhr, "Dielectrophoretic Sorting of Particles and Cells in a Microsystem," *Analytical Chemistry,* vol. 70, pp. 1909-1915, 1998.

[36] H. Gu, M. Duits and F. Mugele, "Droplets formation and merging in two-phase flow microfluidics," *International Journal of Molecular Science,* vol. 12, pp. 2572-2597, 2011.

[37] T. Thorsen, R. W. Roberts, F. H. Arnold and S. R. Quakek, "Dynamic pattern formation in a vesicle-generating microfluidic device," *Physical Review Letters,* vol. 86, no. 18, pp. 4163-4166, 2001.

[38] S. L. Anna, N. Bontoux and H. A. Stone, "Formation of dispersions using "flow focusing" in microchannels," *Applied Physics Letters,* vol. 82, no. 3, pp. 364-366, 2003.

[39] S. Gulati, K. Vijayakumar, W. W. Good and W. L. Tamayo, "Microdroplet formation in rounded flow-focusing junctions," *Microfluidic Nanofluidic,* vol. 20, no. 2, pp. 1-9, 2016.

[40] C. H. Lee, S. Hsiung and G. Lee, "Active micro-mixers utilizing moving wall structures activated pneumatically by buried side chambers," *Journal of Micromechanics and Microengineering,* vol. 17, pp. 1121-1129, 2007.

[41] A. R. Abate, M. B. Romanowsky, J. Agretsi and D. Weitz, "Valve-based flow focusing for drop formation," *Applied Physics Letters,* vol. 92, 2009.

[42] S.-Y. Teh, R. Lin, L.-H. Hung and A. P. Lee, "Droplet Microfluidics," *Lab on a Chip,* vol. 2008, no. 8, pp. 198-220, 2007.

[43] M. S. Shoichet, R. H. Li, M. L. White and S. R. Winn, "Stability of hydrogels used in cell encapsulation: An in vitro comparison oa alignate and agarose.," *Biotechnology and Bioengieering,* vol. 50, pp. 374-381, 1996.

[44] M. M. Sanagi, S. H. Loh, W. N. W. Ibrahim, N. Pourmand, A. Salisu, W. A. W. Ibrahim and I. Ali, "Agarose- and alginate-based biopolymers for sample preparation: Excellent green extraction tools for this century," *Journal of Separation Science,* vol. 39, no. 6, pp. 1152-1159, 2016.

[45] E. M. Ahmed, "Hydrogel: Preparation, characterization, and applications: A review," *Journal of Advanced Research,* vol. 6, no. 2, pp. 105-121, 2015.

[46] N. Monette-Catafard, "High-Throughput Cell Encapsulation in Monodisperse Agarose MIcrocapsules Using a

Microfluidic Device," Master of Science Thesis, University of Ottawa, Ottawa, 2014.

[47] Y. Deng, N. Zhang, L. Zhao, X. Yu, X. Ji, W. Liu, S. Guo, K. Liu and X.-Z. Zhao, "Rapid purification of cell encapsulated hydrogel beads from oil phase to aqueous phase in a microfluidic device," *Lab on a Chip,* vol. 2011, no. 23, pp. 4117-4121, 2011.

[48] S. V. Puttaswamy, S. Sivashankar, R.-J. Chen, C.-K. Chin, H.-Y. Chang and C. H. Liu, "Enhanced cell viability and cell adhesion using low conductivity medium for negative dielectrophoretic cell patterning," *Biotechnology Journal,* vol. 5, pp. 1005-1015, 2010.

[49] GünterFuhr, H. Glasser, T. Müller and T. Schnelle, "Cell manipulation and cultivation under a.c. electric field influence in highly conductive culture media," *Biochimica et Biophysica Acta (BBA) - General Subjects,* vol. 1201, no. 3, pp. 353-360, 1994.

[50] G. Tang, D. Yan, C. Yang, H. Gong, C. Chai and Y. Lam, "Joule heating and its effects on electroosmotic flow in microfluidic channels," in *International MEMS Conference 2006*, 2006.

[51] W. Lee, P. Tseng and D. D. Carlo, Microtechnology for Cell Manipulation and Sorting, Switzerland: Springer International Publishing, 2016.

[52] H.-W. Su, J. L. Prieto and J. Voldman, "Rapid dielectrophoretic characterization of single cells using the dielectrophoretic spring," *Lab on a Chip,* vol. 13, pp. 4109-4117, 2013.

[53] L. Wu, L.-Y. L. Yung and K.-M. Lim, "Dielectrophoretic capture voltage spectrum for measurement of dielectric properties and separation of cancer cells," *Biomicrofluidics,* vol. 014113, pp. 1-10, 2012.

[54] P. R. C. Gascoyne, X.-B. Wang, Y. Huang and F. F. Becker, "Dielectrophoretic Separation of Cancer Cells from Blood," *IEEE Transactions on Industry Applications,* vol. 33, no. 3, pp. 670-678, 2009.

[55] K.-A. Hyun and H.-I. Jung, "Microfluidic devices fo the isolation of circulating rare cells: A focus on affinity-based, dielectrophoresis, and hydrophoresis," *Electrophoresis,* vol. 34, pp. 1028-1041, 2013.

[56] G. A. Truskey, F. Yuan and D. F. Katz, Transport Phenomena in Biological Systems, Second Edition, Pearson, 2009.

[57] D. J. Beebe, G. A.Mensing and G. M.Walker, "Physics and applications of microfluidics in biology," *Annual Review of Biomedical Egineering,* vol. 4, pp. 261-286, 2002.

[58] G. J. Todaro and H. Green, "Quantitative Studies of the Growth of Mouse Embryo Cells in Culture and Their Development into Established Lines," *Journal of Cell Biology,* vol. 17, pp. 299-313, 1963.

[59] P. C. H. Li and D. J. Harrison, "Transport, Manipulation, and Reaction of Biological Cells On-Chip Using Electrokinetic Effects," *Analytical Chemistry,* vol. 69, pp. 1564-1568, 1997.

[60] J. N. Mehrishi and J. Bauer, "Electrophoresis of cells and the biological relevance of surface charge," *Electrophoresis,* vol. 23, pp. 1984-1993, 2002.

[61] Lonza, "Agarose Physical Chemistry," Lonza, [Online]. Available: http://bio.lonza.com/uploads/tx_mwaxmarketingmaterial/Lonza_BenchGuides_SourceBook_Appendix_B_-_Agarose_Physical_Chemistry.pdf.

[62] B10NUMB3R5, "Diameter of NIH/3T3 embryonic fibroblast cell," [Online]. Available: http://bionumbers.hms.harvard.edu//bionumber.aspx?id=108905&ver=1. [Accessed 5 August 2015].

[63] B. Laboratories, "Working with Microspheres," 14 March 2013. [Online]. Available: https://www.bangslabs.com/sites/default/files/imce/docs/TechNote%20201%20Web.pdf.

[64] Y. Huang, S. Joo, M. Duhon, M. Heller, B. Wallace and X. Xu, "Dielectrophoretic Cell Separation and Gene Expression Profiling on Microelectronic Chip Arrays," *Analytical Chemistry,* vol. 74, pp. 3362-3371, 2002.

[65] L. Yang, P. Banada, A. Bhunia and R. Bashir, "Effects of Dielectrophoresis on Growth, Viability and Immuno-reactivity of Listeria Monocytogenes," *Journal of Biological Engineering,* vol. 2, no. 6, pp. 1-14, 2008.

[66] S. Nordling, L. Andersson and P. Hayry, "Separation of T and B lymphocyes by preparative cell electrophoresis," *European Journal of Immunology,* vol. 2, no. 5, pp. 405-410, 1972.

APPENDIX

Photolithography protocol for patterning gold electrodes on glass slides

Adefemi Adeyemi

4/4/2016

Pre-Step

1. Power on Mask Aligner
2. Power on Spin Coater
3. Power on Hot Plate

Main Steps

Step	Procedure	Details
1	Clean	Acetone Ethanol Blow dry
2	Spin	Photoresist = S1813 10s @ 500rpm (Acl = level 1 i.e. 113 rev/min) 30s @ 1000rpm (Acl = level 3 i.e. 339 rev/min) 10s @ 500rpm (Acl = level 3 i.e. 339 rev/min)
3	Pre-Bake	115°C for 1min 20 sec
4	Cool-down	Room temperature for 5 minutes or so
5	Exposure	Expose for 20 sec Wait for 10 sec Expose again for 20 sec
6	Post-Bake	115°C for 1min 20 sec
7	Cool-down	Room temperature for 5 minutes or so
8	Develop	Prepare 36ml DI-H_2O + 4ml TMAH Swirl for 45 sec
9	Rinse	DI-H_2O rinse and N2 blow dry

Post-Step: Clean spin coater with Acetone and Isopropanol

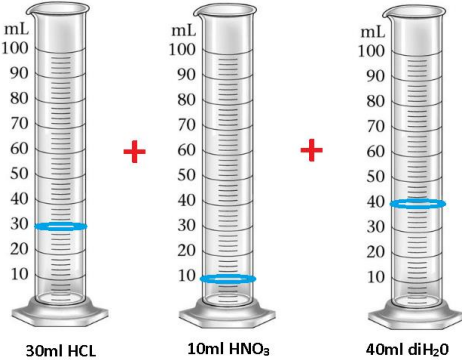**Gold and Chromium etching protocol for glass slides**

Adefemi Adeyemi

4/4/2016

Pre-Step

1. Prepare fume hood: Lay down *acid indicator wipes*, turn on the tap in the hood and leave running for the duration of the experiment. Get a *tweeze*r and keep it in the hood.
2. Prepare containers:
   a. Acid Waste: Take a *1 litre beaker* and fill it halfway with distilled water. Label it with:
      i. Your name
      ii. Date/Time
      iii. ACID WASTE
   b. Dipping/Rinsing: Take *two glass bowls* and label them 'bowl 1' and 'bowl 2'. Use bowl 1 for dipping and bowl 2 for rinsing. Fill bowl 2 halfway with distilled water. Leave bowl 1 empty.
   c. Measuring: Take *two or three measuring cylinders*
3. Put on the appropriate **GLOVES, LAB COAT, PROTECTIVE EYEWEAR, PROTECTIVE SHOES**

Main Steps

Step	Procedure	Details
1	Gold Etching	Step 1: Prepare Aqua regia solution *30ml HCL + 10ml HNO$_3$ + 40ml deionized H$_2$O* 30ml HCL 10ml HNO$_3$ 40ml diH$_2$0 Step 2: Add mixure to bowl 1. Pour water first, and then HCL together with HNO$_3$.

		Step 3: Dip gold-plated glass slide into Aqua regia solution in bowl 1 making sure that the glass slide is completely immersed. Wait till the golden tinge vanishes completely in the exposed regions. Should take about *15 seconds.*
		Step 4: Promptly take out glass slide from Aqua regia solution in bowl 1 and dip in bowl 2 (for rinsing).
		Step 5: Repeat steps 3 and 4 for up to five glass slides if you have that many.
		Step 6: Take glass slide out of bowl 2 and gently wash top-to-bottom, front-and-back with distilled water from the splash bottle.
		Step 7: Blow dry with N_2 air
		Step 8: Dump waste Aqua regia solution in bowl 1 into acid waste beaker and clean/blow-dry bowl 1 for the next step. Bowl 2 remains as it is.
2	Chromium Etching	Step 1: Pour about 60ml of chromium etchant (commercially sold) into bowl 1
		Step 2: Dip glass slide in till the greyish tinge of chromium completely disappears. It takes about *one minute*.
		Step 3: Promptly take glass slide out of bowl 1 and dip into bowl 2
		Step 4: Repeat steps 2 and 3 for up to five glass slides if you have that many.
		Step 5: Take glass slide out of bowl 2 and gently wash top-to-bottom,

		front-and-back with water from the splash bottle.
		Step 6: Blow dry with N_2 air
		Step 7: Dump waste chromium etchant from bowl 1 into the acid waste beaker and clean/blow-dry bowl 1 for the next step. Bowl 2 remains as it is.
3	Developer Removal	Step 1: Pour about 60ml of 1165 photoresist developer into bowl 1
		Step 2: Dip glass slide in and swirl bowl around gently for about 2 minutes
		Step 3: Take glass slide out of bowl 2 and gently wash top-to-bottom, front-and-back with water from the splash bottle.
		Step 4: Blow dry with N_2 air
		Step 5: Dump waste 1165 developer from bowl 1 into the organic waste container.

Post-Steps

- Dump waste water content of bowl 2 into the big acid waste container located <u>outside</u> the fume hood.

- Rinse/wash all bowls/measuring cylinders appropriately

- Collect all acid indicator wipes and examine them for spills. If spills found, place them in the fume hood sink directly under the running tap and let it soak for 5 minutes. Afterwards, squeeze and dump in regular garbage container after.

- Leave the acid waste beaker in fume hood for 24 hours and then dump in the big acid waste container outside the fume hood afterwards.

Photolithography protocol for the fabrication of master moulds on silicon wafers

Adefemi Adeyemi

4/4/2016

Pre-Step

1. Power on Mask Aligner
2. Power on Spin Coater
3. Power on Hot Plates. Set hot plate 1 at 65°C and hot plate 2 at 95°C

Main Steps

Step	Procedure	Details
1	Clean (Rinse)	Acetone for 2 min Ethanol for 2 min Blow dry
2	Pre-dry	115°C for 2 mins
3	Plasma	150W for 5 mins
		Dummy Layer
4	Spin	Photoresist = SU8-10 10s @ 500rpm (Acl = level 1 i.e. 300 rev/min) 60s @ 3000rpm (Acl = level 3 i.e. 1000 rev/min) 10s @ 0rpm (Acl = level 3 i.e. 300 rev/min)
5	Pre-Bake	65°C for 1mins 95°C for 5mins (Prepare mask aligner while waiting)
6	Cool down	Room temperature for 5 minutes or so
7	Exposure	10 sec
8	Post-Bake	65°C for 1mins 95°C for 2mins
9	Cool down	Room temperature for 5 minutes or so
10	Develop	Use SU-8 Developer Swirl in bowl for 2 mins

11	Rinse and blow-dry	Use Isopropanol (splash on wafer from bottle) Blow dry with N_2
12	Heat-dry	150°C for 5 mins (ramp up temperature slowly)
13	Cool down	Room temperature for 5 minutes or so
14	Plasma	150W for 5 mins
Main Layer		
15	Spin	Photoresist = SU8-2050 Use program **M** 10s @ 500rpm (Acl = level 1 i.e. 113 rev/min) 30s @ 1500rpm (Acl = level 3 i.e. 339 rev/min) - for 100um depth 10s @ 500rpm (Acl = level 3 i.e. 339 rev/min)
16	Pre-Bake	65°C for 5mins 95°C for 10mins (Prepare mask aligner while waiting, put masks)
	Cool down	Room temperature for 5 minutes or so
17	Exposure	13 Sec
18	Post-Bake	65°C for 2mins 95°C for 9mins
19	Cool down	Room temperature for 5 minutes or so
20	Develop	Use SU-8 Developer. 3 Steps. • Swirl in bowl 1 for 6 mins • Swirl in bowl 2 for 2 mins • Sprinkle on wafer from bottle
21	Blow-dry	Blow dry with N_2
22	Heat-dry	150°C for 15 mins
23	Cool down	Room temperature for 5 minutes or so

Post-Steps

Clean spin coater with Acetone and Isopropanol

Adefemi Adeyemi

8/6/2017

**Electrode Fabrication for EP Sorting Devices**
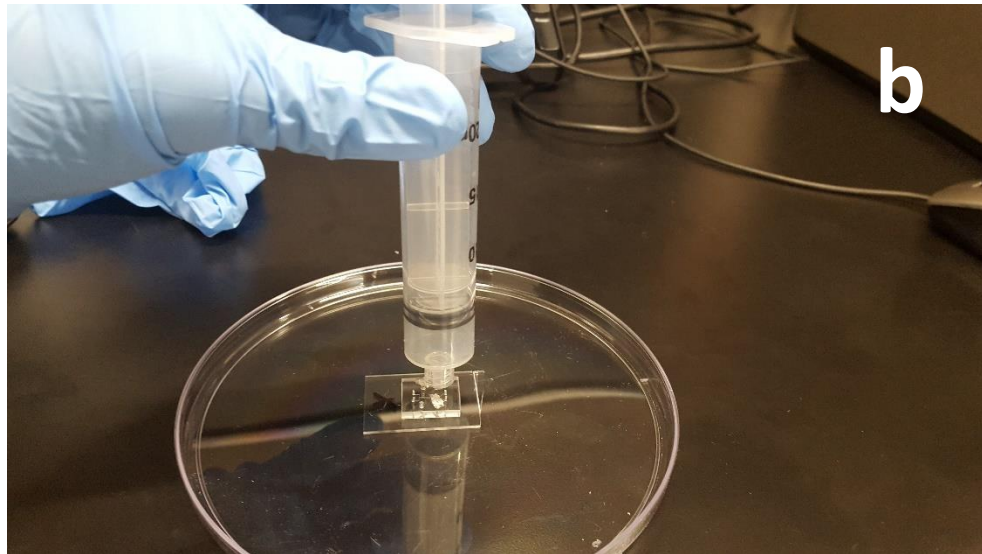
Method 1

1. Place two small Cerrolow 117 alloy pieces over the punched holes of the PDMS that are dedicated for electrodes. Ideally the punched holes should be 1.25mm wide (See figure a).
2. Place in an oven set at 70°C for 2-3 mins for alloy to melt. Although the melting temperature of Cerrolow 117 alloy is 47 °C, it melts faster by subjecting it to a much higher temperature.
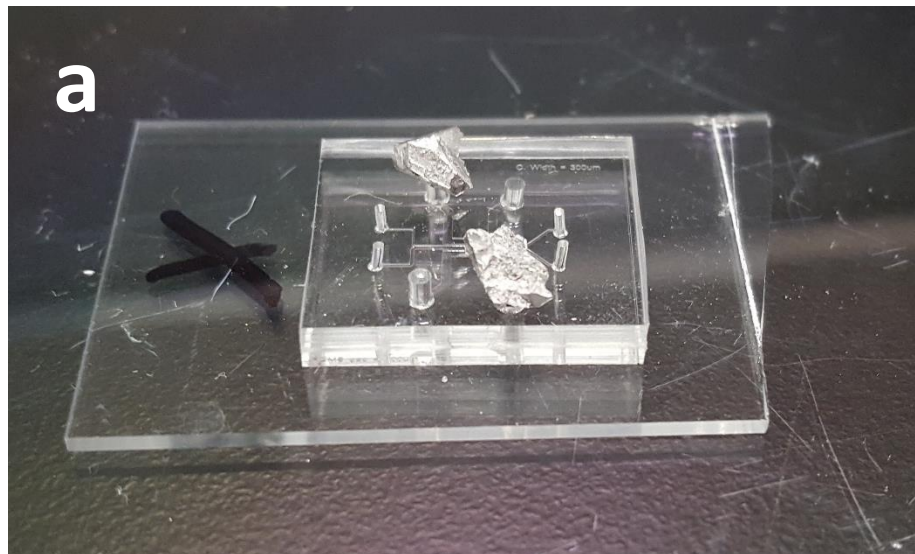
3. Once the alloy has melted, remove the device quickly from the oven
4. Promptly place an syringe over the opposite end of the electrode channel and calmly apply suction (See figure b). The melted allow should gently fill the channel.
5. Next step is to add contact wire. Before the alloy solidifies (from experience, this can take from 30 seconds up to a minute), dip a thin wire into one of the punched holes in either ends of the channel. Make sure the wire is in contact with the molten allow. As the alloy solidifies, the wire should bond to the alloy.
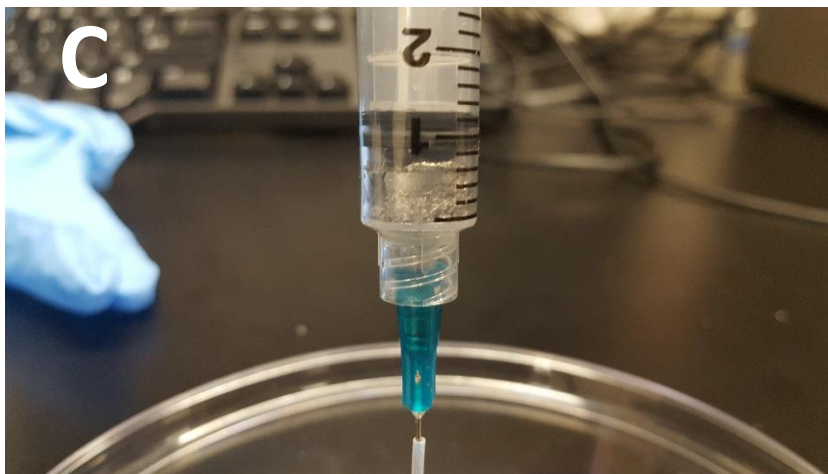
6. Repeat step 5 for the second contact wire (usually, both wires should be inserted at the same time)

Method 2

1. Placed some crushed pieces of alloy in syringe
2. Add a needle to the syringe.
3. Insert the needle to a 1.25mm tube (outer diameter) and glue the exterior of the needle to the interior of the tube – see figure C

4. Insert the other end of the tube into the 1.25mm punched hole meant for electrode access
5. Carefully place the setup (Figure d) in an oven at 70ºC for about 2 to 3 mins. However, it is recommended to inspect every one minute.
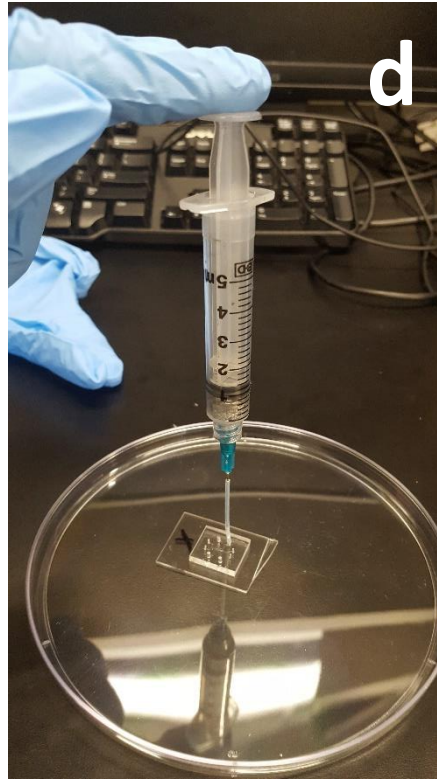
6. While the setup is in the oven, the outer edges of the alloy in the syringe should melt, and the molten alloy should flow through the needle and the tubing into the channel, filling the entire channel and slightly flowing out from the opposite end of the electrode channel.
7. Once it is observed that the alloy is flowing out from the opposite end, withdraw setup from the oven, and carefully pull out the tubing ensure the molten alloy in the syringe does not drip out and spill on the device
8. Promptly insert contact wires into the molten alloy settling over the punched holes and wait for the alloy to solidify.
9. The finished product should look like that shown in figure e below

e